

# 1 Erosion of somatic tissue identity with loss of the X-linked

## 2 intellectual disability factor KDM5C

3

4 Katherine M. Bonefas<sup>1,2</sup>, Ilakkia Venkatachalam<sup>2,3</sup>, and Shigeki Iwase<sup>2</sup>.

5 1. Neuroscience Graduate Program, University of Michigan Medical School, Ann Arbor, MI, 48109, USA.

6      2. Department of Human Genetics, Michigan Medicine, University of Michigan Medical School, Ann Arbor,  
7           MI, 48109, USA.

8 3. Genetics and Genomics Graduate Program, University of Michigan, Ann Arbor, MI, 48109, USA.

## 9 Abstract

10 Mutations in numerous chromatin-modifying enzymes cause neurodevelopmental disorders (NDDs)  
11 with unknown mechanisms. Loss of repressive chromatin regulators can lead to the aberrant transcription  
12 of tissue-specific genes outside of their intended context, however the mechanisms and consequences  
13 of their dysregulation are largely unknown. Here, we examine how lysine demethylase 5c (KDM5C), an  
14 eraser of histone 3 lysine 4 di and tri-methylation (H3K4me2/3) that is mutated in Claes-Jensen X-linked  
15 intellectual disability, contributes to tissue identity. We found male *Kdm5c* knockout (-KO) mice, which  
16 recapitulate key human neurological phenotypes, aberrantly express many liver, muscle, ovary, and testis  
17 genes within the amygdala and hippocampus. Gonad-enriched genes misexpressed in the *Kdm5c*-KO  
18 brain are unique to germ cells, indicating an erosion of the soma-germline boundary. Germline genes are  
19 typically decommissioned in somatic lineages in the post-implantation epiblast, yet *Kdm5c*-KO epiblast-like  
20 cells (EpiLCs) aberrantly expressed key regulators of germline identity and meiosis, including *Dazl* and  
21 *Stra8*. Characterizing germline gene misexpression in males and female mutants revealed germline gene  
22 repression is sexually dimorphic, with female EpiLCs requiring a higher dose of KDM5C to maintain germline  
23 gene suppression. Using a comprehensive list of mouse germline-enriched genes, we found KDM5C is  
24 selectively recruited to a subset of germline gene promoters that contain CpG islands (CGIs) to facilitate  
25 DNA CpG methylation (CpGme) during ESC to EpiLC differentiation. However, late stage spermatogenesis  
26 genes devoid of promoter CGIs can also become activated in *Kdm5c*-KO cells via ectopic activation by RFX  
27 transcription factors. Together, these data demonstrate KDM5C's fundamental role in tissue identity and  
28 indicate that KDM5C acts as a brake against runaway activation of germline developmental programs in  
29 somatic lineages.

## 30 Introduction

31 A single genome holds the instructions to generate the myriad of cell types found within an organism.  
32 This is, in part, accomplished by chromatin regulators that can either promote or impede lineage-specific  
33 gene expression through DNA and histone modifications<sup>1–5</sup>. Human genetic studies revealed mutations in  
34 chromatin regulators are a major cause of neurodevelopmental disorders (NDDs)<sup>6</sup> and many studies have  
35 identified their importance for regulating brain-specific transcriptional programs. Loss of chromatin regulators  
36 can also result in the ectopic expression of tissue-specific genes outside of their target environment, such  
37 as the misexpression of liver-specific genes within adult neurons<sup>7</sup>. However, the mechanisms underlying  
38 ectopic gene expression and its impact upon neurodevelopment are poorly understood.

39 To elucidate the role of tissue identity in chromatin-linked NDDs, it is essential to first characterize the  
40 nature of the dysregulated genes and the molecular mechanisms governing their de-repression. Here we  
41 focus on lysine demethylase 5C (KDM5C, also known as SMCX or JARID1C), which erases histone 3 lysine  
42 4 di- and trimethylation (H3K4me2/3), a permissive chromatin modification enriched at gene promoters<sup>8</sup>.  
43 Pathogenic mutations in the X chromosome gene *KDM5C* cause Intellectual Developmental Disorder, X-  
44 linked, Syndromic, Claes-Jensen Type (MRXSCJ, OMIM: 300534). MRXSCJ is more common and severe  
45 in males and its neurological phenotypes include intellectual disability, seizures, aberrant aggression, and  
46 autistic behaviors<sup>9–11</sup>. Male *Kdm5c* knockout (-KO) mice recapitulate key MRXSCJ phenotypes, including  
47 hyperaggression, increased seizure propensity, social deficits, and learning impairments<sup>12–14</sup>. RNA sequenc-  
48 ing (RNA-seq) of the *Kdm5c*-KO hippocampus revealed ectopic expression of some germline genes within  
49 the brain<sup>13</sup>. However, it is unclear if other tissue-specific genes are aberrantly transcribed with KDM5C loss,  
50 at what point in development germline gene misexpression begins, and what mechanisms underlie their  
51 dysregulation.

52 Distinguishing between germ cells and somatic cells is a key feature of multicellularity<sup>15</sup> that occurs  
53 during early embryogenesis in many metazoans<sup>16</sup>. In mammals, chromatin regulators are crucial for  
54 decommissioning germline genes during the transition from naïve to primed pluripotency. Initially, germline  
55 gene promoters gain repressive histone H2A lysine 119 monoubiquitination (H2AK119ub1)<sup>17</sup> and histone  
56 H3 lysine 9 trimethylation (H3K9me3)<sup>17,18</sup> in embryonic stem cells (ESCs) and are then decorated with  
57 DNA CpG methylation (CpGme) in post-implantation epiblast cells<sup>18–21</sup>. The contribution of KDM5C to this  
58 process remains unclear. Additionally, studies on germline gene repression have primarily been conducted  
59 in males and focused on select marker genes important for early germ cell development, given the lack of a  
60 comprehensive list for germline-enriched genes. Therefore, it is unknown if the mechanism of repression  
61 differs between sexes or for different classes of germline genes, e.g. meiotic versus spermatid differentiation  
62 genes.

63 To illuminate KDM5C's role in tissue identity, here we characterized the aberrant expression of tissue-  
64 enriched genes within the *Kdm5c*-KO brain and epiblast-like stem cells (EpiLCs), an *in vitro* model of the

65 post-implantation embryo. We curated a list of mouse germline-enriched genes, which enabled genome-wide  
66 analysis of germline gene silencing mechanisms for the first time. To illuminate the impact of sex upon  
67 germline gene suppression, we characterized germline transcripts expressed in male and female *Kdm5c*  
68 mutants. Based on the data presented below, we propose KDM5C plays a fundamental, sexually dimorphic  
69 role in the development of tissue identity during early embryogenesis, including the establishment of the  
70 soma-germline boundary.

## 71 Results

### 72 Tissue-enriched genes are aberrantly expressed in the *Kdm5c*-KO brain

73 Previous RNA sequencing (RNA-seq) of the adult male *Kdm5c*-KO hippocampus revealed ectopic  
74 expression of some germline genes unique to the testis<sup>13</sup>. It is currently unknown if the testis is the only  
75 tissue type misexpressed in the *Kdm5c*-KO brain. We thus systematically tested whether other tissue-specific  
76 genes are misexpressed in the male brain with constitutive knockout of *Kdm5c* (*Kdm5c*<sup>-y</sup>, 5CKO)<sup>22</sup> by using  
77 a published list of mouse tissue-enriched genes<sup>23</sup>.

78 We found a large proportion of significantly upregulated genes (DESeq2<sup>24</sup>, log2 fold change > 0.5,  
79 q < 0.1) within the male *Kdm5c*-KO amygdala and hippocampus are non-brain, tissue-specific genes  
80 (Amygdala: 21/59 up DEGs, 35.59% ; Hippocampus: 51/183 up DEGs, 27.87%) (Figure 1A-B). For both the  
81 amygdala and hippocampus, the majority of tissue-enriched differentially expressed genes (DEGs) were  
82 testis genes (Figure 1A-B). Even though the testis has the largest total number of tissue-enriched genes  
83 (2,496 genes) compared to any other tissue, testis-biased DEGs were significantly enriched for both brain  
84 regions (Amygdala p = 1.83e-05, Odds Ratio = 5.13; Hippocampus p = 4.26e-11, Odds Ratio = 4.45, Fisher's  
85 Exact Test). An example of a testis-enriched gene misexpressed in the *Kdm5c*-KO brain is *FK506 binding*  
86 *protein 6 (Fkbp6)*, a known regulator of PIWI-interacting RNAs (piRNAs) and meiosis<sup>25,26</sup> (Figure 1C).

87 Interestingly, we also observed significant enrichment of ovary-biased genes in both the amygdala and  
88 hippocampus (Amygdala p = 0.00574, Odds Ratio = 18.7; Hippocampus p = 0.048, Odds Ratio = 5.88,  
89 Fisher's Exact) (Figure 1A-B). Ovary-enriched DEGs included *Zygotic arrest 1 (Zar1)*, which sequesters  
90 mRNAs in oocytes for meiotic maturation<sup>27</sup> (Figure 1D). Given that the *Kdm5c*-KO mice we analyzed are  
91 male, these data demonstrate that the ectopic expression of gonad-enriched genes is independent of  
92 organismal sex.

93 Although not consistent across brain regions, we also found significant enrichment of genes biased  
94 towards two non-gonadal tissues - the liver (Amygdala p = 0.04, Odds Ratio = 6.58, Fisher's Exact Test) and  
95 muscles (Hippocampus p = 0.01, Odds Ratio = 6.95, Fisher's Exact Test) (Figure 1A-B). *Apolipoprotein C-I*  
96 (*Apoc1*) a lipoprotein metabolism and transport gene, is among the liver-biased DEG derepressed in both  
97 the hippocampus and amygdala<sup>28</sup> and its brain overexpression has been implicated in Alzheimer's disease<sup>29</sup>

98 (Figure 1E).

99 Analysis of oligo(dT)-primed libraries<sup>22</sup> demonstrates aberrantly expressed mRNAs are polyadenylated  
100 and spliced into mature transcripts in the *Kdm5c*-KO brain (Figure 1C-E). Of note, we observed little to no  
101 dysregulation of brain-enriched genes (Amygdala p = 1, Odds Ratio = 1.22; Hippocampus p = 0.74, Odds  
102 Ratio = 1.22, Fisher's Exact), despite the fact these are brain samples and the brain has the second highest  
103 total number of tissue-enriched genes (708 genes). Altogether, these results suggest the aberrant expression  
104 of tissue-enriched genes within the brain is a major effect of KDM5C loss.

105 **Germline genes are misexpressed in the *Kdm5c*-KO brain**

106 *Kdm5c*-KO brain expresses testicular germline genes<sup>13</sup>, however the testis also contains somatic cells that  
107 support hormone production and germline functions. To determine if *Kdm5c*-KO results in ectopic expression  
108 of somatic testicular genes, we first evaluated the known functions of testicular DEGs through gene ontology.  
109 We found *Kdm5c*-KO testis-enriched DEGs had high enrichment of germline-relevant ontologies, including  
110 spermatid development (GO: 0007286, p.adjust = 6.2e-12) and sperm axoneme assembly (GO: 0007288,  
111 p.adjust = 2.45e-14) (Figure 2A).

112 We then evaluated *Kdm5c*-KO testicular DEG expression in wild-type testes versus testes with germ cell  
113 depletion<sup>30</sup>, which was accomplished by heterozygous *W* and *Wv* mutations in the enzymatic domain of *c-Kit*  
114 (*Kit*<sup>W/Wv</sup>)<sup>31</sup>. Almost all *Kdm5c*-KO testis-enriched DEGs lost expression with germ cell depletion (Figure 2B).  
115 We then assessed testis-enriched DEG expression in a published single cell RNA-seq dataset that identified  
116 cell type-specific markers within the testis<sup>32</sup>. Some *Kdm5c*-KO testis-enriched DEGs were classified as  
117 specific markers for different germ cell developmental stages (e.g. spermatogonia, spermatocytes, round  
118 spermatids, and elongating spermatids), yet none marked somatic cells (Figure 2C). Together, these data  
119 demonstrate that the *Kdm5c*-KO brain aberrantly expresses germline genes but not somatic testicular genes,  
120 reflecting an erosion of the soma-germline boundary.

121 As of yet, research on germline gene silencing mechanisms has focused on a handful of key genes rather  
122 than assessing germline gene suppression genome-wide, due to the lack of a comprehensive gene list.  
123 We therefore generated a list of mouse germline-enriched genes using RNA-seq datasets of *Kit*<sup>W/Wv</sup> mice  
124 that included males and females at embryonic day 12, 14, and 16<sup>33</sup> and adult male testes<sup>30</sup>. We defined  
125 genes as germline-enriched if their expression met the following criteria: 1) their expression is greater than  
126 1 FPKM in wild-type gonads 2) their expression in any non-gonadal tissue of adult wild type mice<sup>23</sup> does  
127 not exceed 20% of their maximum expression in the wild-type germline, and 3) their expression in the germ  
128 cell-depleted gonads, for any sex or time point, does not exceed 20% of their maximum expression in the  
129 wild-type germline. These criteria yielded 1,288 germline-enriched genes (Figure 2D), which was hereafter  
130 used as a resource to globally characterize germline gene misexpression with *Kdm5c* loss (Supplementary  
131 table 1).

132 ***Kdm5c*-KO epiblast-like cells aberrantly express key regulators of germline identity**

133 Germ cells are typically distinguished from somatic cells soon after the embryo implants into the uterine  
134 wall<sup>34,35</sup>, when germline genes are silenced in epiblast stem cells that will form the somatic tissues<sup>36</sup>. This  
135 developmental time point can be modeled *in vitro* through differentiation of naïve embryonic stem cells  
136 (nESCs) into epiblast-like stem cells (EpiLCs) (Figure 3A)<sup>37,38</sup>. While some germline-enriched genes are  
137 also expressed in nESCs and in the 2-cell stage<sup>39–41</sup>, they are silenced as they differentiate into EpiLCs<sup>18,19</sup>.  
138 Therefore, we tested if KDM5C was necessary for the initial silencing of germline genes in somatic lineages  
139 by evaluating the impact of *Kdm5c* loss in male EpiLCs.

140 *Kdm5c*-KO cell morphology during ESC to EpiLC differentiation appeared normal (Figure 3B) and EpiLCs  
141 properly expressed markers of primed pluripotency, such as *Dnmt3b*, *Fgf5*, *Pou3f1*, and *Otx2* (Figure 3C). We  
142 then identified tissue-enriched DEGs in a RNA-seq dataset of wild-type and *Kdm5c*-KO EpiLCs<sup>42</sup> (DESeq2,  
143 log<sub>2</sub> fold change > 0.5, q < 0.1). Similar to the *Kdm5c*-KO brain, we observed general dysregulation of  
144 tissue-enriched genes, with the largest number of genes belonging to the brain and testis, although they  
145 were not significantly enriched (Figure 3D). Using our list of mouse germline-enriched genes assembled  
146 above, we identified 68 germline genes misexpressed in male *Kdm5c*-KO EpiLCs.

147 We then compared EpiLC germline DEGs to those expressed in the *Kdm5c*-KO brain to determine if  
148 germline genes are constitutively dysregulated or change over the course of development. The majority of  
149 germline DEGs were unique to either EpiLCs or the brain, with only *D1Pas1* and *Cyct* shared across all  
150 tissue/cell types (Figure 3E-F). EpiLC germline DEGs had particularly high enrichment of meiosis-related  
151 gene ontologies when compared to the brain (Figure 3G), such as meiotic cell cycle process (GO:1903046,  
152 p.adjust = 2.2e-07) and meiotic nuclear division (GO:0140013, p.adjust = 1.37e-07). While there was  
153 modest enrichment of meiotic gene ontologies in both brain regions, the *Kdm5c*-KO hippocampus primarily  
154 expressed late-stage spermatogenesis genes involved in sperm axoneme assembly (GO:0007288, p.adjust  
155 = 0.00621) and sperm motility (GO:0097722, p.adjust = 0.00612).

156 Notably, DEGs unique to *Kdm5c*-KO EpiLCs included key drivers of germline identity, such as *Stimulated*  
157 *by retinoic acid 8* (*Stra8*: log<sub>2</sub> fold change = 3.73, q = 2.17e-39) and *Deleted in azoospermia like* (*Dazl*:  
158 log<sub>2</sub> fold change = 3.36, q = 3.19e-12) (Figure 3H). These genes are typically expressed when a subset of  
159 epiblast cells become primordial germ cells (PGCs) and again later in life to trigger meiotic gene expression  
160 programs<sup>43–45</sup>. Of note, some germline genes, including *Dazl*, are also expressed in the two-cell embryo<sup>40,46</sup>.  
161 However, we did not see derepression of two-cell stage-specific genes, like *Duxf3* (*Dux*) (log<sub>2</sub> fold change  
162 = -0.282, q = 0.337) and *Zscan4d* (log<sub>2</sub> fold change = 0.25, q = 0.381) (Figure 3H), indicating *Kdm5c*-KO  
163 EpiLCs do not revert back to a 2-cell state. Altogether, *Kdm5c*-KO EpiLCs express key drivers of germline  
164 identity and meiosis while the brain primarily expresses spermiogenesis genes, indicating germline gene  
165 misexpression mirrors germline development during the progression of somatic development.

166 **Female epiblast-like cells have increased sensitivity to germline gene misexpression**  
167 **with *Kdm5c* loss**

168 It is currently unknown if the misexpression of germline genes is influenced by sex, as previous studies  
169 on germline gene repressors have focused on male cells<sup>17,18,20,47,48</sup>. Sex is particularly pertinent in the case  
170 of KDM5C because it partially escapes X chromosome inactivation (XCI), resulting in a higher dosage in  
171 females<sup>49–52</sup>. We therefore explored the impact of chromosomal sex upon germline gene suppression by  
172 comparing their dysregulation in male *Kdm5c* hemizygous knockout (XY *Kdm5c*-KO, XY 5CKO), female  
173 homozygous knockout (XX *Kdm5c*-KO, XX 5CKO), and female heterozygous knockout (XX *Kdm5c*-HET, XX  
174 5CHET) EpiLCs<sup>42</sup>.

175 In EpiLCs, homozygous and heterozygous *Kdm5c* knockout females expressed over double the number  
176 of germline-enriched genes than hemizygous males (Figure 4A). While the majority of germline DEGs in  
177 *Kdm5c*-KO males were also dysregulated in females (74%), many were sex-specific, such as *Tktl2* and *Esx1*  
178 (Figure 4B). We then compared the known functions of germline genes dysregulated only in females, only in  
179 males, or in all samples (Figure 4C). Female-specific germline DEGs were enriched for meiotic (GO:0051321  
180 - meiotic cell cycle) and flagellar (GO:0003341 - cilium movement) functions, while male-specific DEGs had  
181 roles in mitochondrial and cell signaling (GO:0070585 - protein localization to mitochondrion).

182 The majority of germline genes expressed in both sexes were more highly dysregulated in females  
183 compared to males (Figure 4D-F). This increased degree of dysregulation in females, along with the  
184 increased total number of germline genes, indicates females are more sensitive to losing KDM5C-mediated  
185 germline gene suppression. Heightened germline gene dysregulation in females could be due to impaired  
186 XCI in *Kdm5c* mutants<sup>42</sup>, as many spermatogenesis genes lie on the X chromosome<sup>53,54</sup>. However, female  
187 germline DEGs were not biased towards the X chromosome and females had a similar overall proportion  
188 of germline DEGs belonging to the X chromosome as males (XY *Kdm5c*-KO - 10.29%, XX *Kdm5c*-HET -  
189 7.43%, XX *Kdm5c*-KO - 10.59%) (Figure 4G). The majority of germline DEGs instead lie on autosomes for  
190 both male and female *Kdm5c* mutants (Figure 4G). Thus, while female EpiLCs are more prone to germline  
191 gene misexpression with KDM5C loss, it is likely independent of XCI defects.

192 **Germline gene misexpression in *Kdm5c* mutants is independent of germ cell sex**

193 Although many germline genes have shared functions in the male and female germline, e.g. PGC  
194 formation, meiosis, and genome defense, some have unique or sex-biased expression. Therefore, we  
195 wondered if *Kdm5c* mutant males would primarily express sperm genes while mutant females would primarily  
196 express egg genes. To comprehensively assess whether germline gene sex corresponds with *Kdm5c* mutant  
197 sex, we first filtered our list of germline-enriched genes for egg and sperm-biased genes (Figure 4H). We  
198 defined germ cell sex-biased genes as those whose expression in the opposite sex, at any time point, is  
199 no greater than 20% of the gene's maximum expression in a given sex. This criteria yielded 0 egg-biased,

200 0 sperm-biased, and 197 unbiased germline-enriched genes. We found regardless of sex, egg, sperm,  
201 and unbiased germline genes were dysregulated in all *Kdm5c* mutants at similar proportions (Figure 4I-J).  
202 Furthermore, germline genes dysregulated exclusively in either male or female mutants were also not biased  
203 towards their corresponding germ cell sex (Figure 4I). Altogether, these results demonstrate sex differences  
204 in germline gene dysregulation is not due to sex-specific activation of sperm or egg transcriptional programs.

## 205 KDM5C binds to a subset of germline gene promoters during early embryogenesis

206 KDM5C binds to the promoters of several germline genes in embryonic stem cells (ESCs) but not in  
207 neurons<sup>13,55</sup>. However, the lack of a comprehensive list of germline-enriched genes prohibited genome-wide  
208 characterization of KDM5C binding at germline gene promoters. Thus, it is unclear if KDM5C is enriched at  
209 germline gene promoters, what types of germline genes KDM5C regulates, and if its binding is maintained at  
210 any germline genes in neurons.

211 To address these questions, we analyzed KDM5C chromatin immunoprecipitation followed by DNA  
212 sequencing (ChIP-seq) datasets in EpiLCs<sup>42</sup> and primary forebrain neuron cultures (PNCs)<sup>12</sup> (MACS2 q  
213 < 0.1, fold enrichment > 1, and removal of false-positive peaks in *Kdm5c*-KO). EpiLCs had a higher total  
214 number of high-confidence KDM5C peaks than PNCs (EpiLCs: 5,808, PNCs: 1,276). KDM5C was primarily  
215 localized to gene promoters in both cell types (promoters = transcription start site (TSS) ± 500 bp, EpiLCs:  
216 4,190, PNCs: 745), although PNCs showed increased localization to non-promoter regions (Figure 5A).

217 The majority of promoters bound by KDM5C in PNCs were also bound in EpiLCs (513 shared promoters),  
218 however a large portion of gene promoters were bound by KDM5C only in EpiLCs (3,677 EpiLC only  
219 promoters) (Figure 5B). Genes bound by KDM5C in both PNCs and EpiLCs were enriched for functions  
220 involving nucleic acid turnover, such as deoxyribonucleotide metabolic process (GO:0009262, p.adjust =  
221 8.28e-05) (Figure 5C). Germline ontologies were enriched only in EpiLC-specific, KDM5C-bound promoters,  
222 such as meiotic nuclear division (GO: 0007127 p.adjust = 6.77e-16) (Figure 5C). There were no significant  
223 ontologies for PNC-specific KDM5C target genes. Using our mouse germline gene list, we observed evident  
224 KDM5C signal around the TSS of many germline genes in EpiLCs, but not in PNCs (Figure 5D). Based  
225 on our ChIP-seq peak cut-off criteria, KDM5C was highly enriched at 211 germline gene promoters in  
226 EpiLCs (16.4% of all germline genes) (Figure 5E). Of note, KDM5C was only bound to about one third  
227 of RNA-seq DEG promoters unique to EpiLCs or the brain (EpiLC only DEGs: 34.9%, Brain only DEGs:  
228 30%) (Supplementary figure 1A-C). Representative examples of EpiLC DEGs bound and unbound by  
229 KDM5C in EpiLCs are *Dazl* and *Stra8*, respectively (Figure 5F). However, the four of the five germline genes  
230 dysregulated in both EpiLCs and the brain were bound by KDM5C in EpiLCs (*D1Pas1*, *Hsf2bp*, *Cyct*, and  
231 *Stk31*) (Supplementary figure 1A). Together, these results demonstrate KDM5C is recruited to a subset  
232 of germline genes in EpiLCs, including meiotic genes, but does not directly regulate germline genes in  
233 neurons. Furthermore, the majority of germline mRNAs expressed in *Kdm5c*-KO cells are dysregulated  
234 independent of direct KDM5C recruitment to their gene promoters, however genes dysregulated across

235 *Kdm5c*-KO development are often direct KDM5C targets.

236 Many germline-specific genes are suppressed by the polycomb repressive complex 1.6 (PRC1.6), which  
237 contains transcription factor heterodimers E2F6/DP1 and MGA/MAX that respectively bind E2F and E-  
238 box motifs within germline gene promoters<sup>58</sup>. PRC1.6 members may recruit KDM5C to germline gene  
239 promoters<sup>13</sup>, given their association with KDM5C in HeLa cells and ESCs<sup>46,59</sup>. We thus used HOMER<sup>60</sup> to  
240 identify transcription factor motifs enriched at KDM5C-bound or unbound germline gene promoters (TSS ±  
241 500 bp, q-value < 0.1). MAX and E2F6 binding sites were significantly enriched at germline genes bound by  
242 KDM5C in EpiLCs (MAX q-value: 0.0068, E2F6 q-value: 0.0673, E2F q-value: 0.0917), but not at germline  
243 genes unbound by KDM5C (Figure 5G). One third of KDM5C-bound promoters contained the consensus  
244 sequence for either E2F6 (E2F, 5'-TCCCCG-3'), MGA (E-box, 5'-CACGTG-3'), or both, but only 17% of  
245 KDM5C-unbound genes contained these motifs (Figure 5H). KDM5C-unbound germline genes were instead  
246 enriched for multiple RFX transcription factor binding sites (RFX q-value < 0.0001, RFX2 q-value < 0.0001,  
247 RFX5 q-value < 0.0001) (Figure 5I, Supplementary figure 1D). RFX transcription factors bind X-box motifs<sup>61</sup>  
248 to promote ciliogenesis<sup>62,63</sup> and among them is RFX2, a central regulator of post-meiotic spermatogenesis<sup>64,65</sup>.  
249 Although *Rfx2* is also not a direct target of KDM5C (Supplementary figure 1E), RFX2 mRNA is derepressed  
250 in *Kdm5c*-KO EpiLCs (Figure 5J). Thus, RFX2 is a candidate transcription factor for driving the ectopic  
251 expression of many KDM5C-unbound germline genes in *Kdm5c*-KO cells.

## 252 **KDM5C is recruited to CpG islands at germline promoters to facilitate *de novo* DNA 253 methylation**

254 Previous work found two germline gene promoters have a marked reduction in DNA CpG methylation  
255 (CpGme) in the *Kdm5c*-KO adult hippocampus<sup>13</sup>. Since histone 3 lysine 4 di- and trimethylation (H3K4me2/3)  
256 impede *de novo* CpGme<sup>66,67</sup>, KDM5C's removal of H3K4me2/3 may be required to suppress germline  
257 genes. However, KDM5C's catalytic activity was recently shown to be dispensable for suppressing *Dazl* in  
258 undifferentiated ESCs<sup>46</sup>. To reconcile these observations, we hypothesized KDM5C erases H3K4me2/3 to  
259 promote the initial placement of CpGme at germline gene promoters in EpiLCs.

260 To test this hypothesis, we first characterized KDM5C's expression as naïve ESCs differentiate into  
261 EpiLCs (Figure 6A). While *Kdm5c* mRNA steadily decreased from 0 to 48 hours of differentiation (Figure  
262 6B), KDM5C protein initially increased from 0 to 24 hours but then decreased to near knockout levels by 48  
263 hours (Figure 6C). We then characterized KDM5C's substrates (H3K4me2/3) at germline gene promoters  
264 with *Kdm5c* loss using published ChIP-seq datasets<sup>22,42</sup>. *Kdm5c*-KO samples showed a marked increase in  
265 H3K4me2 in EpiLCs (Figure 6D) and H3K4me3 in the amygdala (Figure 6E) around the TSS of germline  
266 genes. Together, these data suggest KDM5C acts during the transition between ESCs and EpiLCs to remove  
267 H3K4me2/3 at germline gene promoters.

268 Germline genes accumulate CpG methylation (CpGme) at CpG islands (CGIs) during the transition

269 from naïve to primed pluripotency<sup>19,21,68</sup>. We first examined how many of our germline-enriched genes had  
270 promoter CGIs (TSS ± 500 bp) using the UCSC genome browser<sup>69</sup>. Notably, out of 1,288 germline-enriched  
271 genes, only 356 (27.64%) had promoter CGIs (Figure 6F). CGI-containing germline genes had higher  
272 enrichment of meiotic gene ontologies compared to CGI-free genes, including meiotic nuclear division  
273 (GO:0140013, p.adjust = 2.17e-12) and meiosis I (GO:0007127, p.adjust = 3.91e-10) (Figure 6G). Germline  
274 genes with promoter CGIs were more highly expressed than CGI-free genes across spermatogenesis  
275 stages, with highest expression in meiotic spermatocytes (Figure 6H). Contrastingly, CGI-free genes only  
276 displayed substantial expression in post-meiotic round spermatids (Figure 6H). Although only a minor portion  
277 of germline gene promoters contained CGIs, CGIs strongly determined KDM5C's recruitment to germline  
278 genes ( $p = 2.37e-67$ , Odds Ratio = 17.8, Fisher's exact test), with 79.15% of KDM5C-bound germline gene  
279 promoters harboring CGIs (Figure 6F).

280 To assess how KDM5C loss impacts initial CpGme placement at germline gene promoters, we performed  
281 whole genome bisulfite sequencing (WGBS) in male wild-type and *Kdm5c*-KO ESCs and 96-hour extend  
282 EpiLCs (exEpiLCs), when germline genes reach peak methylation levels<sup>18</sup> (Figure 6I). We first identified  
283 which germline gene promoters significantly gained CpGme in wild-type cells during nESC to exEpiLCs  
284 differentiation (methylKit<sup>70</sup>,  $q < 0.01$ ,  $|methylation\ difference| > 25\%$ , TSS ± 500 bp). In wild-type cells, the  
285 majority of germline genes gained substantial CpGme at their promoter during differentiation (60.08%),  
286 regardless if their promoter contained a CGI (Figure 6J).

287 We then identified promoters differentially methylated in wild-type versus *Kdm5c*-KO exEpiLCs (methylKit,  
288  $q < 0.01$ ,  $|methylation\ difference| > 25\%$ , TSS ± 500 bp). Of the 48,882 promoters assessed, 274 promoters  
289 were significantly hypomethylated and 377 promoters were significantly hypermethylated with KDM5C  
290 loss (Supplementary figure 2A). Many promoters hyper- and hypomethylated in *Kdm5c*-KO exEpiLCs  
291 belonged to genes with unknown functions. 10.22% of hypomethylated promoters belonged to germline  
292 genes and germline-relevant ontologies are significantly enriched, such as meiotic nuclear division (GO:  
293 0140013, p.adjust = 0.012) (Supplementary figure 2B). Approximately half of all germline gene promoters  
294 hypomethylated in *Kdm5c*-KO exEpiLCs are direct targets of KDM5C in EpiLCs (13 out of 28 hypomethylated  
295 promoters).

296 Promoters that showed the most robust loss of CpGme in *Kdm5c*-KO exEpiLCs (lowest q-values) harbored  
297 CGIs (Figure 6K). CGI promoters, but not CGI-free promoters, had a significant reduction in CpGme with  
298 KDM5C loss as a whole (Figure 6L) (Non-CGI promoters  $p = 0.0846$ , CGI promoters  $p = 0.0081$ , Mann-  
299 Whitney U test). Significantly hypomethylated promoters included germline genes consistently dysregulated  
300 across multiple *Kdm5c*-KO RNA-seq datasets<sup>13</sup>, such as *D1PAS1* (methylation difference = -60.03%, q-value  
301 = 3.26e-153) and *NAA11* (methylation difference = -42.45%, q-value = 1.44e-38) (Figure 6M). Surprisingly,  
302 we observed only a modest reduction in CpGme at *Dazl*'s promoter (methylation difference = -6.525%,  
303 q-value = 0.0159) (Figure 6N). Altogether, these results demonstrate KDM5C is recruited to germline gene  
304 CGIs in EpiLCs to promote CpGme at germline gene promoters. Furthermore, this suggests while KDM5C's

305 catalytic activity is required for the repression of some germline genes, CpGme can be placed at others even  
306 with elevated H3K4me2/3 around the TSS.

## 307 Discussion

308 In the above study, we demonstrate KDM5C's pivotal role in the development of tissue identity. We first  
309 characterized tissue-enriched genes expressed within the mouse *Kdm5c*-KO brain and identified substantial  
310 derepression of testis, liver, muscle, and ovary-enriched genes. Testis genes significantly enriched within the  
311 *Kdm5c*-KO amygdala and hippocampus are specific to the germline and absent in somatic cells. *Kdm5c*-KO  
312 epiblast-like cells (EpiLCs) aberrantly express key drivers of germline identity and meiosis, including *Dazl* and  
313 *Stra8*, while the adult brain primarily expresses genes important for late spermatogenesis. We demonstrated  
314 that although sex did not influence whether sperm or egg-specific genes were misexpressed, female EpiLCs  
315 have heightened germline gene de-repression with KDM5C loss. Germline genes can become aberrantly  
316 expressed in *Kdm5c*-KO cells via indirect mechanisms, such as activation through ectopic RFX transcription  
317 factors. Finally, we found KDM5C is dynamically regulated during ESC to EpiLC differentiation to promote  
318 long-term germline gene silencing through DNA methylation at CpG islands. Therefore, we propose KDM5C  
319 plays a fundamental role in the development of tissue identity during early embryogenesis, including the  
320 establishment of the soma-germline boundary. By systematically characterizing KDM5C's role in germline  
321 gene repression, we unveiled unique mechanisms governing the misexpression of distinct germline gene  
322 classes within somatic lineages. Ultimately, these data provide molecular footholds which can be exploited to  
323 test the overarching contribution of ectopic germline gene expression upon neurodevelopment.

324 By comparing *Kdm5c* mutant males and females, we revealed germline gene suppression is sexually  
325 dimorphic. Female EpiLCs are more severely impacted by loss of KDM5C-mediated germline gene suppression,  
326 yet this difference is not due to the increased number of germline genes on the X chromosome<sup>53,54</sup>.  
327 Increased germline gene misexpression in females may be related to females having a higher dose of  
328 KDM5C than males, due to its escape from XCI<sup>49–52</sup>. Intriguingly, heterozygous knockout females (*Kdm5c*<sup>-/+</sup>)  
329 also had over double the number of germline DEGs than hemizygous knockout males (*Kdm5c*<sup>0/0</sup>), even  
330 though their expression of KDM5C should be roughly equivalent to that of wild-type males (*Kdm5c*<sup>+/+</sup>).  
331 Males could partially compensate for KDM5C's loss via the Y-chromosome homolog, KDM5D. However,  
332 KDM5D exhibits weaker demethylase activity than KDM5C<sup>8</sup> and has not been reported to regulate germline  
333 gene expression. Altogether, these results demonstrate germline gene silencing mechanisms differ between  
334 males and females, which warrants further study to elucidate the biological ramifications and underlying  
335 mechanisms.

336 We found KDM5C is largely dispensable for promoting normal gene expression during development, yet  
337 is critical for suppressing ectopic developmental programs. It is important to note that while we highlighted  
338 KDM5C's repression of germline genes, some germline-enriched genes like *Dazl* are also expressed at the 2-

339 cell stage and in the inner cell mass/naïve ESCs for their role in pluripotency and self-renewal<sup>41,46,71,72</sup>. These  
340 “self-renewal” germline genes are then silenced during ESC differentiation into epiblast stem cells/EpiLCs<sup>18,19</sup>.  
341 We found that while *Kdm5c*-KO EpiLCs express *Dazl*, they did not express 2-cell-specific genes like *Zscan4c*.  
342 These data suggest the 2-cell-like state reported in *Kdm5c*-KO ESCs<sup>46</sup> likely reflects KDM5C’s primary  
343 role in germline gene repression. Germline gene misexpression in *Kdm5c*-KO EpiLCs may indicate they  
344 are differentiating into primordial germ cell-like cells (PGCLCs)<sup>34,35,37</sup>. Yet, *Kdm5c*-KO EpiLCs had normal  
345 cellular morphology and properly expressed markers for primed pluripotency, including *Otx2* which blocks  
346 EpiLC differentiation into PGCs/PGCLCs<sup>73</sup>. In addition to unimpaired EpiLC differentiation, *Kdm5c*-KO gross  
347 brain morphology is overall normal<sup>12</sup> and hardly any brain-specific genes were significantly dysregulated in  
348 the amygdala and hippocampus. Thus, ectopic germline gene expression occurs in conjunction with overall  
349 proper somatic differentiation in *Kdm5c*-KO animals.

350 Our work provides novel insight into the cross-talk between H3K4me2/3 and CpGme, which are gen-  
351 erally mutually exclusive<sup>74</sup>. In EpiLCs, loss of KDM5C binding at a subset of germline gene promoters,  
352 e.g. *D1Pas1*, strongly impaired promoter CGI methylation and resulted in their long-lasting de-repression into  
353 adulthood. Removal of H3K4me2/3 at CGIs is a plausible mechanism for KDM5C-mediated germline gene  
354 suppression<sup>13,55</sup>, given H3K4me2/3 can oppose DNMT3 activity<sup>66,67</sup>. However, emerging work indicates  
355 many histone-modifying enzymes have non-catalytic functions that influence gene expression, sometimes  
356 even more potently than their catalytic roles<sup>75,76</sup>. Indeed, KDM5C’s catalytic activity was recently found to be  
357 dispensible for repressing *Dazl* in ESCs<sup>46</sup>. In our study, *Dazl*’s promoter still gained CpGme in *Kdm5c*-KO  
358 exEpiLCs, even with elevated H3K4me2. *Dazl* and a few other germline genes employ multiple repressive  
359 mechanisms to facilitate CpGme, such as DNMT3A/B recruitment via E2F6 and MGA<sup>17,18,47,48</sup>. This suggests  
360 alternative silencing mechanisms are sufficient to recruit DNMT3s to some germline CGIs, while others may  
361 require KDM5C-mediated H3K4me removal to overcome promoter CGI escape from CpGme<sup>74,77</sup>. These  
362 results also suggest the requirement for KDM5C’s catalytic activity can change depending upon the locus  
363 and developmental stage, even for the same class of genes. However, further experiments are required to  
364 determine if catalytically inactive KDM5C can suppress germline genes at later developmental stages.

365 By generating a comprehensive list of mouse germline-enriched genes, we were able to reveal distinct  
366 derepressive mechanisms governing early versus late-stage germline developmental programs. Previous  
367 work on germline gene silencing has focused on genes with promoter CGIs<sup>19,74</sup>, and indeed the major-  
368 ity of KDM5C targets in EpiLCs were germ cell identity genes harboring CGIs. However, over 70% of  
369 germline-enriched gene promoters lacked CGIs, including the many KDM5C-unbound germline genes  
370 that are de-repressed in *Kdm5c*-KO cells. CGI-free, KDM5C-unbound germline genes were primarily  
371 late-stage spermatogenesis genes and significantly enriched for RFX2 binding sites, a central regulator  
372 of spermiogenesis<sup>64,65</sup>. These data suggest that once activated during early embryogenesis, drivers of  
373 germline identity like *Rfx2*, *Stra8*, and *Dazl* turn on downstream germline programs, ultimately culminating in  
374 the expression of spermiogenesis genes in the adult *Kdm5c*-KO brain. Therefore, we propose KDM5C is

375 recruited via promoter CGIs to act as a brake against runaway activation of germline-specific programs.  
376 The above work provides the mechanistic foundation for KDM5C-mediated repression of tissue and  
377 germline-specific genes. However, the contribution of these ectopic, tissue-specific genes towards *Kdm5c*-  
378 KO neurological impairments is still unknown. In addition to germline genes, we also identified significant  
379 enrichment of muscle and liver-biased transcripts within the *Kdm5c*-KO brain. Intriguingly, select liver and  
380 muscle-biased DEGs do have known roles within the brain, such as the liver-enriched lipid metabolism gene  
381 *Apolipoprotein C-I (Apoc1)*<sup>28</sup>. *APOC1* dysregulation is implicated in Alzheimer's disease in humans<sup>29</sup> and  
382 overexpression of *Apoc1* in the mouse brain can impair learning and memory<sup>78</sup>. KDM5C may therefore be  
383 crucial for neurodevelopment by fine-tuning the expression of tissue-enriched, dosage-sensitive genes like  
384 *Apoc1*.

385 Given that germline genes have no known functions within the brain, their impact upon neurodevelopment  
386 is currently unknown. In *C. elegans*, somatic misexpression of germline genes via loss of *Retinoblastoma*  
387 (*Rb*) homologs results in enhanced piRNA signaling and ectopic P granule formation in neurons<sup>79,80</sup>. Ectopic  
388 testicular germline transcripts have also been observed in a variety of cancers, including brain tumors in  
389 *Drosophila* and mammals<sup>81,82</sup> and shown to promote cancer progression<sup>83–85</sup>. Intriguingly, mouse models  
390 and human cells for other chromatin-linked NDDs also display impaired soma-germline demarcation<sup>86–88</sup>,  
391 such as mutations in DNA methyltransferase 3b (DNMT3B), H3K9me1/2 methyltransferases G9A/GLP,  
392 and methyl-CpG -binding protein 2 (MECP2). Recently, the transcription factor ZMYM2 (ZNF198), whose  
393 mutation causes neurodevelopmental-craniofacial syndrome with variable renal and cardiac abnormalities  
394 (OMIM #619522), was also shown to repress germline genes by promoting H3K4 methylation removal and  
395 CpGme<sup>89</sup>. Thus, KDM5C is among a growing cohort of neurodevelopmental disorders that have erosion of  
396 the germline-soma boundary. Further research is required to determine the impact of these germline genes  
397 upon neuronal functions and the extent to which this phenomenon occurs in humans.

## 398 Materials and Methods

### 399 Classifying tissue-enriched and germline-enriched genes

400 Tissue-enriched differentially expressed genes (DEGs) were determined by their classification in a previ-  
401 ously published dataset from 17 male and female mouse tissues<sup>23</sup>. This study defined tissue expression as  
402 greater than 1 Fragments Per Kilobase of transcript per Million mapped read (FPKM) and tissue enrichment  
403 as at least 4-fold higher expression than any other tissue.

404 We curated a list of germline-enriched genes using an RNA-seq dataset from wild-type and germline-  
405 depleted (*Kit<sup>W/Wv</sup>*) male and female mouse embryos from embryonic day 12, 14, and 16<sup>33</sup>, as well as adult  
406 male testes<sup>30</sup>. Germline-enriched genes met the following criteria: 1) their expression is greater than 1  
407 FPKM in wild-type germline 2) their expression in any wild-type somatic tissues<sup>23</sup> does not exceed 20%

408 of maximum expression in wild-type germline, and 3) their expression in the germ cell-depleted (*Kit*<sup>W/W<sup>v</sup></sup>)  
409 germline, for any sex or time point, does not exceed 20% of maximum expression in wild-type germline. We  
410 defined sperm and egg-biased genes as those whose expression in the opposite sex, at any time point, is no  
411 greater than 20% of the gene's maximum expression in a given sex. Genes that did not meet this threshold  
412 for either sex were classified as 'unbiased'.

## 413 Cell culture

414 We utilized our previously established cultures of male wild-type and *Kdm5c* knockout (-KO)  
415 embryonic stem cells<sup>42</sup>. Sex was confirmed by genotyping *Uba1/Uba1y* on the X and Y chromo-  
416 somes with the following primers: 5'-TGGATGGTGTGCCAATG-3', 5'-CACCTGCACGTTGCCCTT-  
417 3'. Deletion of *Kdm5c* exons 11 and 12, which destabilize KDM5C protein<sup>12</sup>, was confirmed  
418 through the primers 5'-ATGCCCATATTAAGAGTCCCTG-3', 5'-TCTGCCTTGATGGACTGTT-3', and  
419 5'-GGTTCTAACACTCACATAGTG-3'.

420 Embryonic stem cells (ESCs) and epiblast-like cells were cultured using previously established  
421 methods<sup>38</sup>. Briefly, ESCs were initially cultured in primed ESC (pESC) media consisting of KnockOut  
422 DMEM (Gibco#10829–018), fetal bovine serum (Gibco#A5209501), KnockOut serum replacement  
423 (Invitrogen#10828–028), Glutamax (Gibco#35050-061), Anti-Anti (Gibco#15240-062), MEM Non-essential  
424 amino acids (Gibco#11140-050), and beta-mercaptoethanol (Sigma#M7522). They were then transitioned  
425 into ground-state, "naïve" ESCs (nESCs) by culturing for four passages in N2B27 media containing  
426 DMEM/F12 (Gibco#11330–032), Neurobasal media (Gibco#21103–049), Gluamax (Gibco#35050-061),  
427 Anti-Anti (Gibco#15240-062), N2 supplement (Invitrogen#17502048), and B27 supplement without vitamin  
428 A (Invitrogen#12587-010), and beta-mercaptoethanol (Sigma#M7522). Both pESC and nESC media  
429 were supplemented with 3 µM GSK3 inhibitor CHIR99021 (Sigma #SML1046-5MG), 1 µM MEK inhibitor  
430 PD0325901 (Sigma #PZ0162-5MG), and 1,000 units/mL leukemia inhibitory factor (LIF, Millipore#ESG1107).  
431 nESCs were differentiated into epiblast-like cells (EpiLCs, 48 hours) and extendend EpiLCs (exEpiLCs,  
432 96 hours) by culturing in N2B27 media containing DMEM/F12, Neurobasal media, Gluamax, Anti-Anti, N2  
433 supplement, B27 supplement (Invitrogen#17504044), and beta-mercaptoethanol supplemented with 10  
434 ng/mL fibroblast growth factor 2 (FGF2, R&D Biotechne 233-FB), and 20 ng/mL activin A (R&D Biotechne  
435 338AC050CF), as previously described<sup>38</sup>.

## 436 Real time quantitative PCR (RT-qPCR)

437 nESCs were differentiated into EpiLCs as described above. Cells were lysed with Tri-reagent BD (Sigma  
438 #T3809) at 0, 24, and 48 hours of differentiation. RNA was phase separated with 0.1 uL/uL 1-bromo-3-  
439 chloropropane (Sigma #B9673) and then precipitated with isopropanol (Sigma #I9516) and ethanol puri-  
440 fied. For each sample, 2 µg of RNA was reverse transcribed using the ProtoScript II Reverse transcriptase kit

441 from New England Biolabs (NEB #M0368S) and primed with oligo dT. Expression of *Kdm5c* was detected us-  
442 ing the primers 5'-CCCATGGAGGCCAGAGAATAAG-3' 5'-CTCAGCGGATAAGAGAATTGCTAC-3' and nor-  
443 malized to TBP using the primers 5'-TTCAGAGGATGCTCTAGGGAAGA-3' 5'-CTGTGGAGTAAGTCCTGTGCC-  
444 3' with the Power SYBR™ Green PCR Master Mix (ThermoFisher #4367659).

#### 445 **Western Blot**

446 Total protein was extracted during nESC to EpiLC differentiation at 0, 24, and 48 hours by sonicating cells  
447 at 20% amplitude for 15 seconds in 2X SDS sample buffer, then boiling at 100°C for 10 minutes. Proteins  
448 were separated on a 7.5% SDS page gel, transferred overnight onto a fluorescent membrane, blotted for  
449 rabbit anti-KDM5C (in house, 1:500) and mouse anti-DAXX (Santa Cruz #(H-7): sc-8043, 1:500) and imaged  
450 using the LiCor Odyssey CLx system. Band intensity was quantified using ImageJ.

#### 451 **RNA sequencing (RNA-seq) data analysis**

452 After ensuring read quality via FastQC (v0.11.8), reads were then mapped to the mm10 *Mus musculus*  
453 genome (Gencode) using STAR (v2.5.3a), during which we removed duplicates and kept only uniquely  
454 mapped reads. Count files were generated by FeatureCounts (Subread v1.5.0), and BAM files were  
455 converted to bigwigs using deeptools (v3.1.3) and visualized by the UCSC genome browser<sup>69</sup>. RStudio  
456 (v3.6.0) was then used to analyze counts files by DESeq2 (v1.26.0)<sup>24</sup> to identify differentially expressed  
457 genes (DEGs) with a q-value (p-adjusted via FDR/Benjamini–Hochberg correction) less than 0.1 and a log2  
458 fold change greater than 0.5. For all DESeq2 analyses, log2 fold changes were calculated with IfcShrink  
459 using the ashR package<sup>90</sup>. MA-plots were generated by ggpibr (v0.6.0), and Eulerr diagrams were generated  
460 by eulerr (v6.1.1). Boxplots and scatterplots were generated by ggpibr (v0.6.0) and ggplot2 (v3.3.2). The  
461 Upset plot was generated via the package UpSetR (v1.4.0)<sup>91</sup>. Gene ontology (GO) analyses were performed  
462 by the R package enrichPlot (v1.16.2) using the biological processes setting and compareCluster.

#### 463 **Chromatin immunoprecipitation followed by DNA sequencing (ChIP-seq) data analysis**

464 ChIP-seq reads were aligned to mm10 using Bowtie1 (v1.1.2) allowing up to two mismatches. Only  
465 uniquely mapped reads were used for analysis. Peaks were called using MACS2 software (v2.2.9.1) using  
466 input BAM files for normalization, with filters for a q-value < 0.1 and a fold enrichment > 1. We removed  
467 “black-listed” genomic regions that often give aberrant signals. Common peak sets were obtained in R via  
468 DiffBind<sup>92</sup> (v3.6.5). In the case of KDM5C ChIP-seq, *Kdm5c*-KO peaks false-positive peaks were then  
469 removed from wild-type samples using bedtools (v2.25.0). Peak proximity to genomic loci was determined  
470 by ChIPSeeker<sup>93</sup> (v1.32.1). Gene ontology (GO) analyses were performed by the R package enrichPlot  
471 (v1.16.2) using the biological processes setting and compareCluster. Enriched motifs were identified using  
472 HOMER<sup>60</sup> to search for known motifs within 500 base pairs of the transcription start site. Average binding

473 across genes was visualized using deeptools (v3.1.3). Bigwigs were visualized using the UCSC genome  
474 browser<sup>69</sup>.

## 475 **CpG island (CGI) analysis**

476 Locations of CpG islands were determined through the mm10 UCSC genome browser CpG island track<sup>69</sup>,  
477 which classified CGIs as regions that have greater than 50% GC content, are larger than 200 base pairs,  
478 and have a ratio of CG dinucleotides observed over the expected amount greater than 0.6. CGI genomic  
479 coordinates were then annotated using ChIPseeker<sup>93</sup> (v1.32.1) and filtered for ones that lie within promoters  
480 of germline-enriched genes (TSS ± 500).

## 481 **Whole genome bisulfite sequencing (WGBS)**

482 Genomic DNA (gDNA) from naïve ESCs and extended EpiLCs was extracted using the Wizard Genomic  
483 DNA Purification Kit (Promega A1120), following the instructions for Tissue Culture Cells. gDNA from  
484 two wild-types and two *Kdm5c*-KOs of each cell type was sent to Novogene for WGBS using the Illumina  
485 NovaSeq X Plus platform and sequenced for 150bp paired-end reads (PE150). All samples had greater  
486 than 99% bisulfite conversion rates. Reads were adapter and quality trimmed with Trim Galore (v0.6.10)  
487 and aligned to the mm10 genome using Bismark<sup>94</sup> (v0.22.1). Analysis of differential methylation at germline  
488 gene promoters was performed using methylKit<sup>70</sup> (v1.28.0) with a minimum coverage of 3 paired reads, a  
489 percentage greater than 25% or less than -25%, and q-value less than 0.01. methylKit was also used to  
490 calculate average percentage methylation at germline gene promoters. Methylation bedgraph tracks were  
491 generated via Bismark and visualized using the UCSC genome browser<sup>69</sup>.

## 492 **Data availability**

### 493 **WGBS in wild-type and *Kdm5c*-KO ESCs and exEpiLCs**

494 Raw fastq files are deposited in the Sequence Read Archive (SRA) <https://www.ncbi.nlm.nih.gov/sra>  
495 under the bioProject XXX

## 496 **Published datasets**

497 All published datasets are available at the Gene Expression Omnibus (GEO) <https://www.ncbi.nlm.nih.gov/geo/>. Published RNA-seq datasets analyzed in this study included the male wild-type and *Kdm5c*-KO  
498 adult amygdala and hippocampus<sup>22</sup> (available at GEO: GSE127722). Male and female wild-type, *Kdm5c*-KO,  
499 and *Kdm5c*-HET EpiLCs<sup>42</sup> are available at GEO: GSE96797.

501 Previously published ChIP-seq experiments included KDM5C binding in wild-type and *Kdm5c*-KO  
502 EpiLCs<sup>42</sup> (available at GEO: GSE96797) and mouse primary neuron cultures (PNCs) from the cortex

503 and hippocampus<sup>12</sup> (available at GEO: GSE61036). ChIP-seq of histone 3 lysine 4 dimethylation (H3K4me2)  
504 in male wild-type and *Kdm5c*-KO EpiLCs<sup>42</sup> is also available at GEO: GSE96797. ChIP-seq of histone 3 lysine  
505 4 trimethylation (H3K4me3) in wild-type and *Kdm5c*-KO male amygdala<sup>22</sup> are available at GEO: GSE127817.

## 506 Data analysis

507 Scripts used to generate the results, tables, and figures of this study are available via the GitHub  
508 repository: XXX

## 509 Acknowledgements

510 We thank Drs. Sundeep Kalantry, Milan Samanta, and Rebecca Malcore for providing protocols and  
511 expertise in culturing mouse ESCs and EpiLCs, as well as providing the wild-type and *Kdm5c*-KO ESCs  
512 used in this study. We thank Dr. Jacob Mueller for his insight in germline gene regulation and directing us to  
513 the germline-depleted mouse models. We also thank Drs. Gabriel Corfas, Kenneth Kwan, Natalie Tronson,  
514 Michael Sutton, Stephanie Bielas, Donna Martin, and the members of the Iwase, Sutton, Bielas, and Martin  
515 labs for helpful discussions and critiques of the data. We thank members of the University of Michigan  
516 Reproductive Sciences Program for providing feedback throughout the development of this work. This work  
517 was supported by grants from the National Institutes of Health (NIH) (National Institute of Neurological  
518 Disorders and Stroke: NS089896, 5R21NS104774, and NS116008 to S.I.), Farrehi Family Foundation Grant  
519 (to S.I.), the University of Michigan Career Training in Reproductive Biology (NIH T32HD079342, to K.M.B.),  
520 the NIH Early Stage Training in the Neurosciences Training Grant (NIH T32NS076401 to K.M.B.), and the  
521 Michigan Predoctoral Training in Genetics Grant (NIH T32GM007544, to I.V.)

## 522 Author contributions

523 K.M.B. and S.I. conceived the study and designed the experiments. I.V. generated the ESC and exEpiLC  
524 WGBS data. K.M.B performed the data analysis and all other experiments. K.M.B and S.I. wrote and edited  
525 the manuscript.

## 526 References

- 527 1. Strahl, B.D., and Allis, C.D. (2000). The language of covalent histone modifications. *Nature* **403**,  
528 41–45. <https://doi.org/10.1038/47412>.
- 529 2. Jenuwein, T., and Allis, C.D. (2001). Translating the Histone Code. *Science* **293**, 1074–1080.  
530 <https://doi.org/10.1126/science.1063127>.

- 531 3. Lewis, E.B. (1978). A gene complex controlling segmentation in *Drosophila*. *Nature* *276*, 565–570.  
532 <https://doi.org/10.1038/276565a0>.
- 533 4. Kennison, J.A., and Tamkun, J.W. (1988). Dosage-dependent modifiers of polycomb and antennapedia  
534 mutations in *Drosophila*. *Proc. Natl. Acad. Sci. U.S.A.* *85*, 8136–8140. <https://doi.org/10.1073/pnas.85.21.8136>.
- 535 5. Kassis, J.A., Kennison, J.A., and Tamkun, J.W. (2017). Polycomb and Trithorax Group Genes in  
536 *Drosophila*. *Genetics* *206*, 1699–1725. <https://doi.org/10.1534/genetics.115.185116>.
- 537 6. Gabriele, M., Lopez Tobon, A., D'Agostino, G., and Testa, G. (2018). The chromatin basis of  
538 neurodevelopmental disorders: Rethinking dysfunction along the molecular and temporal axes. *Prog  
Neuropsychopharmacol Biol Psychiatry* *84*, 306–327. <https://doi.org/10.1016/j.pnpbp.2017.12.013>.
- 539 7. Schaefer, A., Sampath, S.C., Intrator, A., Min, A., Gertler, T.S., Surmeier, D.J., Tarakhovsky, A.,  
540 and Greengard, P. (2009). Control of cognition and adaptive behavior by the GLP/G9a epigenetic  
suppressor complex. *Neuron* *64*, 678–691. <https://doi.org/10.1016/j.neuron.2009.11.019>.
- 541 8. Iwase, S., Lan, F., Bayliss, P., De La Torre-Ubieta, L., Huarte, M., Qi, H.H., Whetstine, J.R., Bonni, A.,  
542 Roberts, T.M., and Shi, Y. (2007). The X-Linked Mental Retardation Gene SMCX/JARID1C Defines a  
Family of Histone H3 Lysine 4 Demethylases. *Cell* *128*, 1077–1088. <https://doi.org/10.1016/j.cell.2007.02.017>.
- 543 9. Claes, S., Devriendt, K., Van Goethem, G., Roelen, L., Meireleire, J., Raeymaekers, P., Cassiman,  
544 J.J., and Fryns, J.P. (2000). Novel syndromic form of X-linked complicated spastic paraparesis. *Am J  
Med Genet* *94*, 1–4.
- 545 10. Jensen, L.R., Amende, M., Gurok, U., Moser, B., Gimmel, V., Tzschach, A., Janecke, A.R., Tariverdian,  
546 G., Chelly, J., Fryns, J.P., et al. (2005). Mutations in the JARID1C gene, which is involved in  
transcriptional regulation and chromatin remodeling, cause X-linked mental retardation. *Am J Hum  
Genet* *76*, 227–236. <https://doi.org/10.1086/427563>.
- 547 11. Carmignac, V., Nambot, S., Lehalle, D., Callier, P., Moortgat, S., Benoit, V., Ghoumid, J., Delobel,  
548 B., Smol, T., Thuillier, C., et al. (2020). Further delineation of the female phenotype with KDM5C  
disease causing variants: 19 new individuals and review of the literature. *Clin Genet* *98*, 43–55.  
<https://doi.org/10.1111/cge.13755>.
- 549 12. Iwase, S., Brookes, E., Agarwal, S., Badeaux, A.I., Ito, H., Vallianatos, C.N., Tomassy, G.S., Kasza, T.,  
550 Lin, G., Thompson, A., et al. (2016). A Mouse Model of X-linked Intellectual Disability Associated with  
Impaired Removal of Histone Methylation. *Cell Reports* *14*, 1000–1009. <https://doi.org/10.1016/j.celrep.2015.12.091>.

- 551 13. Scandaglia, M., Lopez-Atalaya, J.P., Medrano-Fernandez, A., Lopez-Cascales, M.T., Del Blanco, B.,  
552 Lipinski, M., Benito, E., Olivares, R., Iwase, S., Shi, Y., et al. (2017). Loss of Kdm5c Causes Spurious  
Transcription and Prevents the Fine-Tuning of Activity-Regulated Enhancers in Neurons. *Cell Rep* **21**,  
47–59. <https://doi.org/10.1016/j.celrep.2017.09.014>.
- 553 14. Bonefas, K.M., Vallianatos, C.N., Raines, B., Tronson, N.C., and Iwase, S. (2023). Sexually Dimorphic  
554 Alterations in the Transcriptome and Behavior with Loss of Histone Demethylase KDM5C. *Cells* **12**,  
637. <https://doi.org/10.3390/cells12040637>.
- 555 15. Devlin, D.K., Ganley, A.R.D., and Takeuchi, N. (2023). A pan-metazoan view of germline-soma  
556 distinction challenges our understanding of how the metazoan germline evolves. *Current Opinion in  
Systems Biology* **36**, 100486. <https://doi.org/10.1016/j.coisb.2023.100486>.
- 557 16. Lehmann, R. (2012). Germline Stem Cells: Origin and Destiny. *Cell Stem Cell* **10**, 729–739.  
558 <https://doi.org/10.1016/j.stem.2012.05.016>.
- 559 17. Endoh, M., Endo, T.A., Shinga, J., Hayashi, K., Farcas, A., Ma, K.W., Ito, S., Sharif, J., Endoh, T.,  
560 Onaga, N., et al. (2017). PCGF6-PRC1 suppresses premature differentiation of mouse embryonic  
stem cells by regulating germ cell-related genes. *eLife* **6**. <https://doi.org/10.7554/eLife.21064>.
- 561 18. Mochizuki, K., Sharif, J., Shirane, K., Uranishi, K., Bogutz, A.B., Janssen, S.M., Suzuki, A., Okuda,  
A., Koseki, H., and Lorincz, M.C. (2021). Repression of germline genes by PRC1.6 and SETDB1  
in the early embryo precedes DNA methylation-mediated silencing. *Nat Commun* **12**, 7020. <https://doi.org/10.1038/s41467-021-27345-x>.
- 563 19. Borgel, J., Guibert, S., Li, Y., Chiba, H., Schübeler, D., Sasaki, H., Forné, T., and Weber, M. (2010).  
Targets and dynamics of promoter DNA methylation during early mouse development. *Nat Genet* **42**,  
564 1093–1100. <https://doi.org/10.1038/ng.708>.
- 565 20. Velasco, G., Hubé, F., Rollin, J., Neuillet, D., Philippe, C., Bouzinba-Segard, H., Galvani, A., Viegas-  
Péquignot, E., and Francastel, C. (2010). Dnmt3b recruitment through E2F6 transcriptional repressor  
mediates germ-line gene silencing in murine somatic tissues. *Proc Natl Acad Sci U S A* **107**, 9281–  
566 9286. <https://doi.org/10.1073/pnas.1000473107>.
- 567 21. Hackett, J.A., Reddington, J.P., Nestor, C.E., Dunican, D.S., Branco, M.R., Reichmann, J., Reik,  
W., Surani, M.A., Adams, I.R., and Meehan, R.R. (2012). Promoter DNA methylation couples  
genome-defence mechanisms to epigenetic reprogramming in the mouse germline. *Development*  
568 **139**, 3623–3632. <https://doi.org/10.1242/dev.081661>.
- 569 22. Vallianatos, C.N., Raines, B., Porter, R.S., Bonefas, K.M., Wu, M.C., Garay, P.M., Collette, K.M.,  
Seo, Y.A., Dou, Y., Keegan, C.E., et al. (2020). Mutually suppressive roles of KMT2A and KDM5C  
in behaviour, neuronal structure, and histone H3K4 methylation. *Commun Biol* **3**, 278. <https://doi.org/10.1038/s42003-020-1001-6>.

- 571 23. Li, B., Qing, T., Zhu, J., Wen, Z., Yu, Y., Fukumura, R., Zheng, Y., Gondo, Y., and Shi, L. (2017). A  
572 Comprehensive Mouse Transcriptomic BodyMap across 17 Tissues by RNA-seq. *Sci Rep* 7, 4200.  
<https://doi.org/10.1038/s41598-017-04520-z>.
- 573 24. Love, M.I., Huber, W., and Anders, S. (2014). Moderated estimation of fold change and dispersion for  
574 RNA-seq data with DESeq2. *Genome Biol* 15, 550. <https://doi.org/10.1186/s13059-014-0550-8>.
- 575 25. Crackower, M.A., Kolas, N.K., Noguchi, J., Sarao, R., Kikuchi, K., Kaneko, H., Kobayashi, E., Kawai, Y.,  
576 Kozieradzki, I., Landers, R., et al. (2003). Essential Role of Fkbp6 in Male Fertility and Homologous  
Chromosome Pairing in Meiosis. *Science* 300, 1291–1295. <https://doi.org/10.1126/science.1083022>.
- 577 26. Xiol, J., Cora, E., Koglgruber, R., Chuma, S., Subramanian, S., Hosokawa, M., Reuter, M., Yang, Z.,  
578 Berninger, P., Palencia, A., et al. (2012). A Role for Fkbp6 and the Chaperone Machinery in piRNA  
Amplification and Transposon Silencing. *Molecular Cell* 47, 970–979. <https://doi.org/10.1016/j.molcel.2012.07.019>.
- 579 27. Cheng, S., Altmeppen, G., So, C., Welp, L.M., Penir, S., Ruhwedel, T., Menelaou, K., Harasimov, K.,  
580 Stützer, A., Blayney, M., et al. (2022). Mammalian oocytes store mRNAs in a mitochondria-associated  
membraneless compartment. *Science* 378, eabq4835. <https://doi.org/10.1126/science.abq4835>.
- 581 28. Rouland, A., Masson, D., Lagrost, L., Vergès, B., Gautier, T., and Bouillet, B. (2022). Role of  
582 apolipoprotein C1 in lipoprotein metabolism, atherosclerosis and diabetes: A systematic review.  
*Cardiovasc Diabetol* 21, 272. <https://doi.org/10.1186/s12933-022-01703-5>.
- 583 29. Leduc, V., Jasmin-Bélanger, S., and Poirier, J. (2010). APOE and cholesterol homeostasis in  
584 Alzheimer's disease. *Trends in Molecular Medicine* 16, 469–477. <https://doi.org/10.1016/j.molmed.2010.07.008>.
- 585 30. Mueller, J.L., Skaletsky, H., Brown, L.G., Zaghlul, S., Rock, S., Graves, T., Auger, K., Warren,  
586 W.C., Wilson, R.K., and Page, D.C. (2013). Independent specialization of the human and mouse X  
chromosomes for the male germ line. *Nat Genet* 45, 1083–1087. <https://doi.org/10.1038/ng.2705>.
- 587 31. Handel, M.A., and Eppig, J.J. (1979). Sertoli Cell Differentiation in the Testes of Mice Genetically  
588 Deficient in Germ Cells. *Biology of Reproduction* 20, 1031–1038. <https://doi.org/10.1095/biolreprod20.5.1031>.
- 589 32. Green, C.D., Ma, Q., Manske, G.L., Shami, A.N., Zheng, X., Marini, S., Moritz, L., Sultan, C.,  
590 Gurczynski, S.J., Moore, B.B., et al. (2018). A Comprehensive Roadmap of Murine Spermatogenesis  
Defined by Single-Cell RNA-Seq. *Dev Cell* 46, 651–667.e10. <https://doi.org/10.1016/j.devcel.2018.07.025>.
- 591 33. Soh, Y.Q., Junker, J.P., Gill, M.E., Mueller, J.L., van Oudenaarden, A., and Page, D.C. (2015). A  
592 Gene Regulatory Program for Meiotic Prophase in the Fetal Ovary. *PLoS Genet* 11, e1005531.  
<https://doi.org/10.1371/journal.pgen.1005531>.

- 593 34. Magnúsdóttir, E., and Surani, M.A. (2014). How to make a primordial germ cell. *Development* *141*,  
594 245–252. <https://doi.org/10.1242/dev.098269>.
- 595 35. Günesdogan, U., Magnúsdóttir, E., and Surani, M.A. (2014). Primordial germ cell specification: A  
596 context-dependent cellular differentiation event [corrected]. *Philos Trans R Soc Lond B Biol Sci* *369*.  
<https://doi.org/10.1098/rstb.2013.0543>.
- 597 36. Bardot, E.S., and Hadjantonakis, A.-K. (2020). Mouse gastrulation: Coordination of tissue patterning,  
598 specification and diversification of cell fate. *Mechanisms of Development* *163*, 103617. <https://doi.org/10.1016/j.mod.2020.103617>.
- 599 37. Hayashi, K., Ohta, H., Kurimoto, K., Aramaki, S., and Saitou, M. (2011). Reconstitution of the  
600 mouse germ cell specification pathway in culture by pluripotent stem cells. *Cell* *146*, 519–532.  
<https://doi.org/10.1016/j.cell.2011.06.052>.
- 601 38. Samanta, M., and Kalantry, S. (2020). Generating primed pluripotent epiblast stem cells: A methodol-  
602 ogy chapter. *Curr Top Dev Biol* *138*, 139–174. <https://doi.org/10.1016/bs.ctdb.2020.01.005>.
- 603 39. Welling, M., Chen, H., Muñoz, J., Musheev, M.U., Kester, L., Junker, J.P., Mischerikow, N., Arbab, M.,  
604 Kuijk, E., Silberstein, L., et al. (2015). DAZL regulates Tet1 translation in murine embryonic stem cells.  
*EMBO Reports* *16*, 791–802. <https://doi.org/10.15252/embr.201540538>.
- 605 40. Macfarlan, T.S., Gifford, W.D., Driscoll, S., Lettieri, K., Rowe, H.M., Bonanomi, D., Firth, A., Singer, O.,  
606 Trono, D., and Pfaff, S.L. (2012). Embryonic stem cell potency fluctuates with endogenous retrovirus  
activity. *Nature* *487*, 57–63. <https://doi.org/10.1038/nature11244>.
- 607 41. Suzuki, A., Hirasaki, M., Hishida, T., Wu, J., Okamura, D., Ueda, A., Nishimoto, M., Nakachi, Y.,  
608 Mizuno, Y., Okazaki, Y., et al. (2016). Loss of MAX results in meiotic entry in mouse embryonic and  
germline stem cells. *Nat Commun* *7*, 11056. <https://doi.org/10.1038/ncomms11056>.
- 609 42. Samanta, M.K., Gayen, S., Harris, C., Maclary, E., Murata-Nakamura, Y., Malcore, R.M., Porter, R.S.,  
610 Garay, P.M., Vallianatos, C.N., Samollow, P.B., et al. (2022). Activation of Xist by an evolutionarily  
conserved function of KDM5C demethylase. *Nat Commun* *13*, 2602. <https://doi.org/10.1038/s41467-022-30352-1>.
- 611 43. Koubova, J., Menke, D.B., Zhou, Q., Capel, B., Griswold, M.D., and Page, D.C. (2006). Retinoic  
acid regulates sex-specific timing of meiotic initiation in mice. *Proc. Natl. Acad. Sci. U.S.A.* *103*,  
612 2474–2479. <https://doi.org/10.1073/pnas.0510813103>.
- 613 44. Lin, Y., Gill, M.E., Koubova, J., and Page, D.C. (2008). Germ Cell-Intrinsic and -Extrinsic Factors  
614 Govern Meiotic Initiation in Mouse Embryos. *Science* *322*, 1685–1687. <https://doi.org/10.1126/science.1166340>.
- 615 45. Endo, T., Mikedis, M.M., Nicholls, P.K., Page, D.C., and De Rooij, D.G. (2019). Retinoic Acid and Germ  
616 Cell Development in the Ovary and Testis. *Biomolecules* *9*, 775. <https://doi.org/10.3390/biom9120775>.

- 617 46. Gupta, N., Yakhou, L., Albert, J.R., Azogui, A., Ferry, L., Kirsh, O., Miura, F., Battault, S., Yamaguchi,  
618 K., Laisné, M., et al. (2023). A genome-wide screen reveals new regulators of the 2-cell-like cell state.  
Nat Struct Mol Biol. <https://doi.org/10.1038/s41594-023-01038-z>.
- 619 47. Pohlers, M., Truss, M., Frede, U., Scholz, A., Strehle, M., Kuban, R.-J., Hoffmann, B., Morkel, M.,  
620 Birchmeier, C., and Hagemann, C. (2005). A Role for E2F6 in the Restriction of Male-Germ-Cell-  
Specific Gene Expression. Current Biology 15, 1051–1057. <https://doi.org/10.1016/j.cub.2005.04.060>.
- 621 48. Dahlet, T., Truss, M., Frede, U., Al Adhami, H., Bardet, A.F., Dumas, M., Vallet, J., Chicher, J.,  
622 Hammann, P., Kottnik, S., et al. (2021). E2F6 initiates stable epigenetic silencing of germline genes  
during embryonic development. Nat Commun 12, 3582. <https://doi.org/10.1038/s41467-021-23596-w>.
- 623 49. Agulnik, A.I., Mitchell, M.J., Mattei, M.G., Borsani, G., Avner, P.A., Lerner, J.L., and Bishop, C.E.  
624 (1994). A novel X gene with a widely transcribed Y-linked homologue escapes X-inactivation in mouse  
and human. Hum Mol Genet 3, 879–884. <https://doi.org/10.1093/hmg/3.6.879>.
- 625 50. Carrel, L., Hunt, P.A., and Willard, H.F. (1996). Tissue and lineage-specific variation in inactive  
X chromosome expression of the murine Smcx gene. Hum Mol Genet 5, 1361–1366. <https://doi.org/10.1093/hmg/5.9.1361>.
- 627 51. Sheardown, S., Norris, D., Fisher, A., and Brockdorff, N. (1996). The mouse Smcx gene exhibits  
developmental and tissue specific variation in degree of escape from X inactivation. Hum Mol Genet  
628 5, 1355–1360. <https://doi.org/10.1093/hmg/5.9.1355>.
- 629 52. Xu, J., Deng, X., and Disteche, C.M. (2008). Sex-Specific Expression of the X-Linked Histone  
Demethylase Gene Jarid1c in Brain. PLoS ONE 3, e2553. <https://doi.org/10.1371/journal.pone.0002553>.
- 631 53. Wang, P.J., McCarrey, J.R., Yang, F., and Page, D.C. (2001). An abundance of X-linked genes  
632 expressed in spermatogonia. Nat Genet 27, 422–426. <https://doi.org/10.1038/86927>.
- 633 54. Khil, P.P., Smirnova, N.A., Romanienko, P.J., and Camerini-Otero, R.D. (2004). The mouse X  
chromosome is enriched for sex-biased genes not subject to selection by meiotic sex chromosome  
634 inactivation. Nat Genet 36, 642–646. <https://doi.org/10.1038/ng1368>.
- 635 55. Al Adhami, H., Vallet, J., Schaal, C., Schumacher, P., Bardet, A.F., Dumas, M., Chicher, J., Hammann,  
636 P., Daujat, S., and Weber, M. (2023). Systematic identification of factors involved in the silencing  
of germline genes in mouse embryonic stem cells. Nucleic Acids Research 51, 3130–3149. <https://doi.org/10.1093/nar/gkad071>.
- 637 56. Hurlin, P.J. (1999). Mga, a dual-specificity transcription factor that interacts with Max and contains a  
T-domain DNA-binding motif. The EMBO Journal 18, 7019–7028. <https://doi.org/10.1093/emboj/18.2.7019>.

- 639 57. Tatsumi, D., Hayashi, Y., Endo, M., Kobayashi, H., Yoshioka, T., Kiso, K., Kanno, S., Nakai, Y., Maeda, I., Mochizuki, K., et al. (2018). DNMTs and SETDB1 function as co-repressors in MAX-mediated repression of germ cell-related genes in mouse embryonic stem cells. *PLoS ONE* *13*, e0205969. <https://doi.org/10.1371/journal.pone.0205969>.
- 640
- 641 58. Stielow, B., Finkernagel, F., Stiewe, T., Nist, A., and Suske, G. (2018). MGA, L3MBTL2 and E2F6 determine genomic binding of the non-canonical Polycomb repressive complex PRC1.6. *PLoS Genet* *14*, e1007193. <https://doi.org/10.1371/journal.pgen.1007193>.
- 642
- 643 59. Tahiliani, M., Mei, P., Fang, R., Leonor, T., Rutenberg, M., Shimizu, F., Li, J., Rao, A., and Shi, Y. (2007). The histone H3K4 demethylase SMCX links REST target genes to X-linked mental retardation. *Nature* *447*, 601–605. <https://doi.org/10.1038/nature05823>.
- 644
- 645 60. Heinz, S., Benner, C., Spann, N., Bertolino, E., Lin, Y.C., Laslo, P., Cheng, J.X., Murre, C., Singh, H., and Glass, C.K. (2010). Simple Combinations of Lineage-Determining Transcription Factors Prime cis-Regulatory Elements Required for Macrophage and B Cell Identities. *Molecular Cell* *38*, 576–589. <https://doi.org/10.1016/j.molcel.2010.05.004>.
- 646
- 647 61. Gajiwala, K.S., Chen, H., Cornille, F., Roques, B.P., Reith, W., Mach, B., and Burley, S.K. (2000). Structure of the winged-helix protein hRFX1 reveals a new mode of DNA binding. *Nature* *403*, 916–921. <https://doi.org/10.1038/35002634>.
- 648
- 649 62. Swoboda, P., Adler, H.T., and Thomas, J.H. (2000). The RFX-Type Transcription Factor DAF-19 Regulates Sensory Neuron Cilium Formation in *C. elegans*. *Molecular Cell* *5*, 411–421. [https://doi.org/10.1016/S1097-2765\(00\)80436-0](https://doi.org/10.1016/S1097-2765(00)80436-0).
- 650
- 651 63. Ashique, A.M., Choe, Y., Karlen, M., May, S.R., Phamluong, K., Solloway, M.J., Ericson, J., and Peterson, A.S. (2009). The Rfx4 Transcription Factor Modulates Shh Signaling by Regional Control of Ciliogenesis. *Sci. Signal.* *2*. <https://doi.org/10.1126/scisignal.2000602>.
- 652
- 653 64. Kistler, W.S., Baas, D., Lemeille, S., Paschaki, M., Seguin-Estevez, Q., Barras, E., Ma, W., Duteyrat, J.-L., Morlé, L., Durand, B., et al. (2015). RFX2 Is a Major Transcriptional Regulator of Spermiogenesis. *PLoS Genet* *11*, e1005368. <https://doi.org/10.1371/journal.pgen.1005368>.
- 654
- 655 65. Wu, Y., Hu, X., Li, Z., Wang, M., Li, S., Wang, X., Lin, X., Liao, S., Zhang, Z., Feng, X., et al. (2016). Transcription Factor RFX2 Is a Key Regulator of Mouse Spermiogenesis. *Sci Rep* *6*, 20435. <https://doi.org/10.1038/srep20435>.
- 656
- 657 66. Otani, J., Nankumo, T., Arita, K., Inamoto, S., Ariyoshi, M., and Shirakawa, M. (2009). Structural basis for recognition of H3K4 methylation status by the DNA methyltransferase 3A ATRX–DNMT3–DNMT3L domain. *EMBO Reports* *10*, 1235–1241. <https://doi.org/10.1038/embor.2009.218>.
- 658

- 659 67. Guo, X., Wang, L., Li, J., Ding, Z., Xiao, J., Yin, X., He, S., Shi, P., Dong, L., Li, G., et al. (2015).  
660 Structural insight into autoinhibition and histone H3-induced activation of DNMT3A. *Nature* **517**,  
640–644. <https://doi.org/10.1038/nature13899>.
- 661 68. Meissner, A., Mikkelsen, T.S., Gu, H., Wernig, M., Hanna, J., Sivachenko, A., Zhang, X., Bernstein,  
662 B.E., Nusbaum, C., Jaffe, D.B., et al. (2008). Genome-scale DNA methylation maps of pluripotent and  
differentiated cells. *Nature* **454**, 766–770. <https://doi.org/10.1038/nature07107>.
- 663 69. Nassar, L.R., Barber, G.P., Benet-Pagès, A., Casper, J., Clawson, H., Diekhans, M., Fischer, C.,  
664 Gonzalez, J.N., Hinrichs, A.S., Lee, B.T., et al. (2023). The UCSC Genome Browser database: 2023  
update. *Nucleic Acids Research* **51**, D1188–D1195. <https://doi.org/10.1093/nar/gkac1072>.
- 665 70. Akalin, A., Kormaksson, M., Li, S., Garrett-Bakelman, F.E., Figueiroa, M.E., Melnick, A., and Mason,  
666 C.E. (2012). methylKit: A comprehensive R package for the analysis of genome-wide DNA methylation  
profiles. *Genome Biol* **13**, R87. <https://doi.org/10.1186/gb-2012-13-10-r87>.
- 667 71. Torres-Padilla, M.-E. (2020). On transposons and totipotency. *Philos Trans R Soc Lond B Biol Sci*  
668 **375**, 20190339. <https://doi.org/10.1098/rstb.2019.0339>.
- 669 72. Yang, M., Yu, H., Yu, X., Liang, S., Hu, Y., Luo, Y., Izsvák, Z., Sun, C., and Wang, J. (2022). Chemical-  
670 induced chromatin remodeling reprograms mouse ESCs to totipotent-like stem cells. *Cell Stem Cell*  
29, 400–418.e13. <https://doi.org/10.1016/j.stem.2022.01.010>.
- 671 73. Zhang, J., Zhang, M., Acampora, D., Vojtek, M., Yuan, D., Simeone, A., and Chambers, I. (2018).  
672 OTX2 restricts entry to the mouse germline. *Nature* **562**, 595–599. <https://doi.org/10.1038/s41586-018-0581-5>.
- 673 74. Weber, M., Hellmann, I., Stadler, M.B., Ramos, L., Pääbo, S., Rebhan, M., and Schübeler, D. (2007).  
674 Distribution, silencing potential and evolutionary impact of promoter DNA methylation in the human  
genome. *Nat Genet* **39**, 457–466. <https://doi.org/10.1038/ng1990>.
- 675 75. Aubert, Y., Egolf, S., and Capell, B.C. (2019). The Unexpected Noncatalytic Roles of Histone Modifiers  
676 in Development and Disease. *Trends in Genetics* **35**, 645–657. <https://doi.org/10.1016/j.tig.2019.06.004>.
- 677 76. Morgan, M.A.J., and Shilatifard, A. (2020). Reevaluating the roles of histone-modifying enzymes  
678 and their associated chromatin modifications in transcriptional regulation. *Nat Genet* **52**, 1271–1281.  
<https://doi.org/10.1038/s41588-020-00736-4>.
- 679 77. Long, H.K., King, H.W., Patient, R.K., Odom, D.T., and Klose, R.J. (2016). Protection of CpG  
islands from DNA methylation is DNA-encoded and evolutionarily conserved. *Nucleic Acids Res* **44**,  
680 6693–6706. <https://doi.org/10.1093/nar/gkw258>.

- 681 78. Abildayeva, K., Berbée, J.F.P., Blokland, A., Jansen, P.J., Hoek, F.J., Meijer, O., Lütjohann, D., Gautier, T., Pillot, T., De Vente, J., et al. (2008). Human apolipoprotein C-I expression in mice impairs learning and memory functions. *Journal of Lipid Research* *49*, 856–869. <https://doi.org/10.1194/jlr.M700518JLR200>.
- 682
- 683 79. Wang, D., Kennedy, S., Conte, D., Kim, J.K., Gabel, H.W., Kamath, R.S., Mello, C.C., and Ruvkun, G. (2005). Somatic misexpression of germline P granules and enhanced RNA interference in retinoblastoma pathway mutants. *Nature* *436*, 593–597. <https://doi.org/10.1038/nature04010>.
- 684
- 685 80. Wu, X., Shi, Z., Cui, M., Han, M., and Ruvkun, G. (2012). Repression of germline RNAi pathways in somatic cells by retinoblastoma pathway chromatin complexes. *PLoS Genet* *8*, e1002542. <https://doi.org/10.1371/journal.pgen.1002542>.
- 686
- 687 81. Nielsen, A.Y., and Gjerstorff, M.F. (2016). Ectopic Expression of Testis Germ Cell Proteins in Cancer and Its Potential Role in Genomic Instability. *Int J Mol Sci* *17*. <https://doi.org/10.3390/ijms17060890>.
- 688
- 689 82. Adebayo Babatunde, K., Najafi, A., Salehipour, P., Modarressi, M.H., and Mobasher, M.B. (2017). Cancer/Testis genes in relation to sperm biology and function. *Iranian Journal of Basic Medical Sciences* *20*. <https://doi.org/10.22038/ijbms.2017.9259>.
- 690
- 691 83. Janic, A., Mendizabal, L., Llamazares, S., Rossell, D., and Gonzalez, C. (2010). Ectopic expression of germline genes drives malignant brain tumor growth in *Drosophila*. *Science* *330*, 1824–1827. <https://doi.org/10.1126/science.1195481>.
- 692
- 693 84. Ghafouri-Fard, S., and Modarressi, M.-H. (2012). Expression of Cancer–Testis Genes in Brain Tumors: Implications for Cancer Immunotherapy. *Immunotherapy* *4*, 59–75. <https://doi.org/10.2217/imt.11.145>.
- 694
- 695 85. Nin, D.S., and Deng, L.-W. (2023). Biology of Cancer-Testis Antigens and Their Therapeutic Implications in Cancer. *Cells* *12*, 926. <https://doi.org/10.3390/cells12060926>.
- 696
- 697 86. Bonefas, K.M., and Iwase, S. (2021). Soma-to-germline transformation in chromatin-linked neurode-698  
developmental disorders? *FEBS J.* <https://doi.org/10.1111/febs.16196>.
- 699 87. Velasco, G., Walton, E.L., Sterlin, D., Hédouin, S., Nitta, H., Ito, Y., Fouyssac, F., Mégarbané, A., Sasaki, H., Picard, C., et al. (2014). Germline genes hypomethylation and expression define a molecular signature in peripheral blood of ICF patients: Implications for diagnosis and etiology. *Orphanet J Rare Dis* *9*, 56. <https://doi.org/10.1186/1750-1172-9-56>.
- 700
- 701 88. Walton, E.L., Francastel, C., and Velasco, G. (2014). Dnmt3b Prefers Germ Line Genes and Cen-  
tromeric Regions: Lessons from the ICF Syndrome and Cancer and Implications for Diseases. *Biology* *(Basel)* *3*, 578–605. <https://doi.org/10.3390/biology3030578>.
- 702

- 703 89. Graham-Paquin, A.-L., Saini, D., Sirois, J., Hossain, I., Katz, M.S., Zhuang, Q.K.-W., Kwon, S.Y.,  
Yamanaka, Y., Bourque, G., Bouchard, M., et al. (2023). ZMYM2 is essential for methylation of  
germline genes and active transposons in embryonic development. *Nucleic Acids Research*, gkad540.  
704 <https://doi.org/10.1093/nar/gkad540>.
- 705 90. Stephens, M. (2016). False discovery rates: A new deal. *Biostat*, kxw041. <https://doi.org/10.1093/biostatistics/kxw041>.
- 707 91. Conway, J.R., Lex, A., and Gehlenborg, N. (2017). UpSetR: An R package for the visualization of  
intersecting sets and their properties. *Bioinformatics* 33, 2938–2940. <https://doi.org/10.1093/bioinformatics/btx364>.
- 709 92. Ross-Innes, C.S., Stark, R., Teschendorff, A.E., Holmes, K.A., Ali, H.R., Dunning, M.J., Brown, G.D.,  
Gojis, O., Ellis, I.O., Green, A.R., et al. (2012). Differential oestrogen receptor binding is associated  
710 with clinical outcome in breast cancer. *Nature* 481, 389–393. <https://doi.org/10.1038/nature10730>.
- 711 93. Yu, G., Wang, L.G., and He, Q.Y. (2015). ChIPseeker: An R/Bioconductor package for ChIP peak  
annotation, comparison and visualization. *Bioinformatics* 31, 2382–2383. <https://doi.org/10.1093/bioinformatics/btv145>.
- 713 94. Krueger, F., and Andrews, S.R. (2011). Bismark: A flexible aligner and methylation caller for Bisulfite-  
714 Seq applications. *Bioinformatics* 27, 1571–1572. <https://doi.org/10.1093/bioinformatics/btr167>.

715 **Figures and Tables**

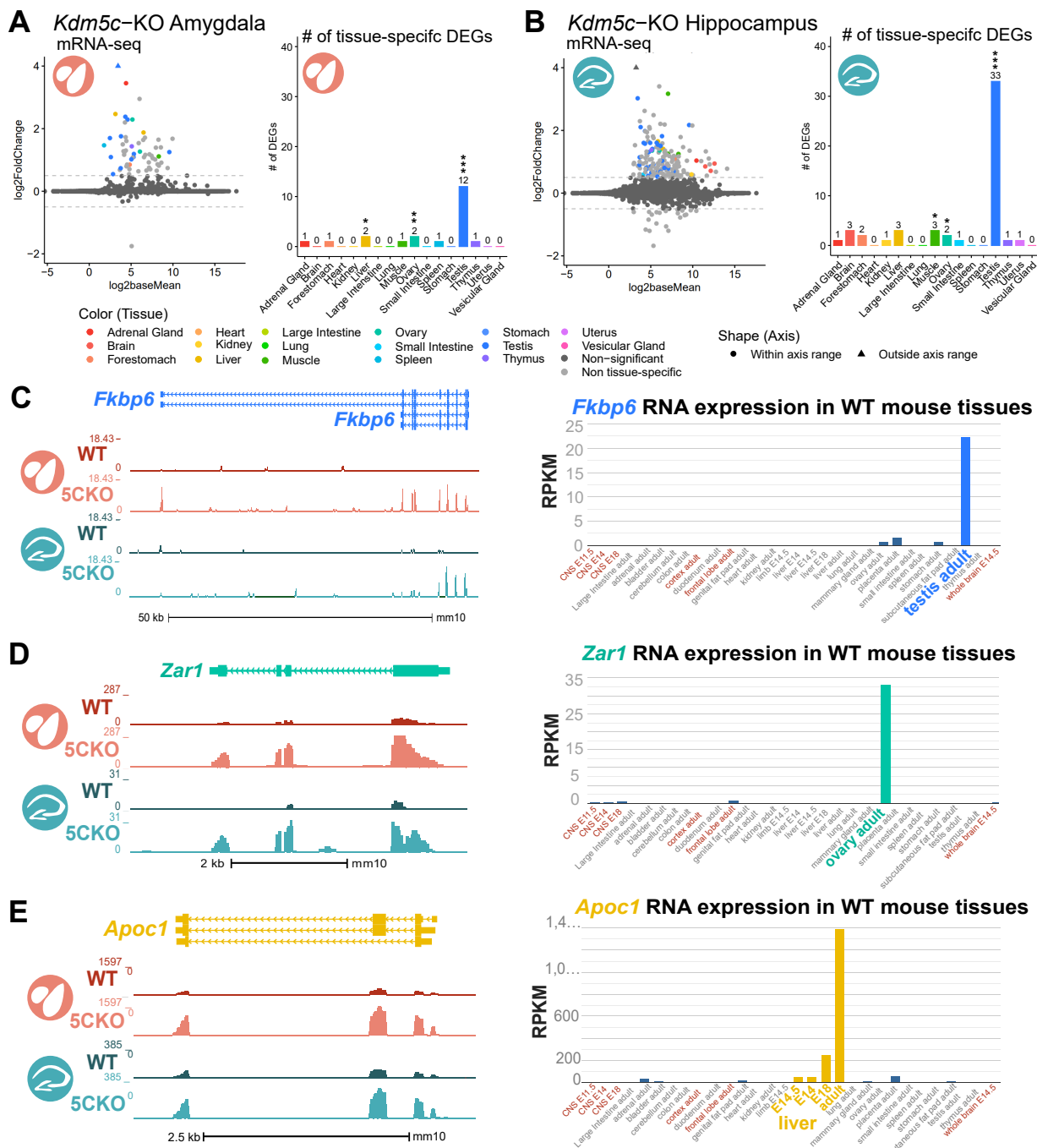


**Figure 1: Tissue-enriched genes are misexpressed in the *Kdm5c*-KO brain.** **A-B.** Expression of tissue-enriched genes (Li et al 2017) in the male *Kdm5c*-KO amygdala (A) and hippocampus (B). Left - MA plot of mRNA-sequencing. Right - Number of tissue-enriched differentially expressed genes (DEGs). \*  $p < 0.05$ , \*\*  $p < 0.01$ , \*\*\*  $p < 0.001$ , Fisher's exact test. **C.** Left - UCSC browser view of an example aberrantly expressed testis-enriched DEG, *FK506 binding protein 6* (*Fkbp6*) in the wild-type (WT) and *Kdm5c*-KO (5CKO) amygdala (red) and hippocampus (teal) (Average,  $n = 4$ ). Right - Expression of *Cyct* in wild-type tissues from NCBI Gene, with testis highlighted in blue and brain tissues highlighted in red. **D.** Left - UCSC browser view of an example ovary-enriched DEG, *Zygotic arrest 1* (*Zar1*). Right - Expression of *Zar1* in wild-type tissues from NCBI Gene, with ovary highlighted in teal and brain tissues highlighted in red. **E.** Left - UCSC browser view of an example liver-enriched DEG, *Apolipoprotein C-I* (*Apoc1*). Right - Expression of *Apoc1* in wild-type tissues from NCBI Gene, with liver highlighted in orange and brain tissues highlighted in red.

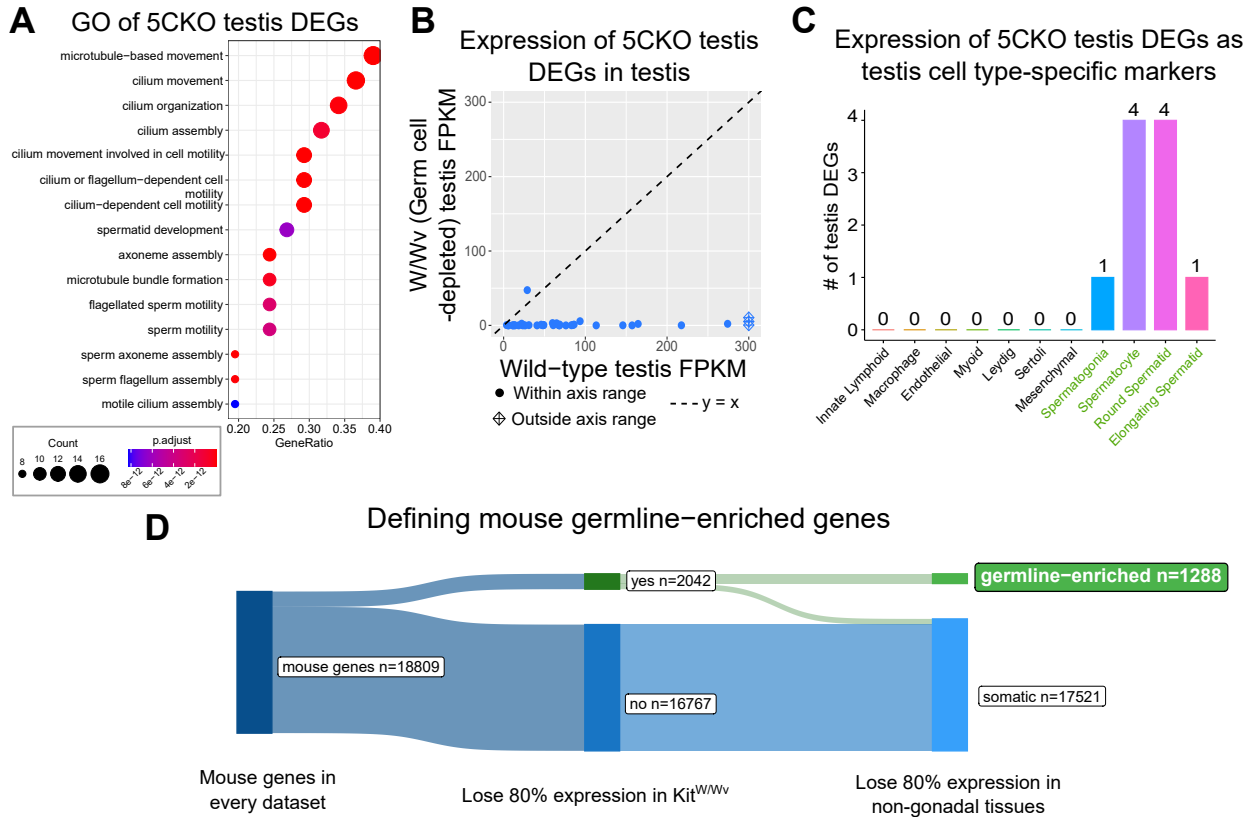


**Figure 2: Aberrant transcription of germline genes in the *Kdm5c*-KO in the brain.** **A.** enrichPlot gene ontology (GO) of *Kdm5c*-KO amygdala and hippocampus testis-enriched DEGs **B.** Expression of testis DEGs in wild-type (WT) testis versus germ cell-depleted (W/Wv) testis (Mueller et al 2013). Expression is in Fragments Per Kilobase of transcript per Million mapped reads (FPKM). **C.** Number of testis DEGs that were classified as cell-type specific markers in a single cell RNA-seq dataset of the testis (Green et al 2018). Germline cell types are highlighted in green, somatic cell types in black. **D.** Sankey diagram of mouse genes filtered for germline enrichment based on their expression in wild-type and W/Wv mice and in adult mouse non-gonadal tissues (Li et al 2017).

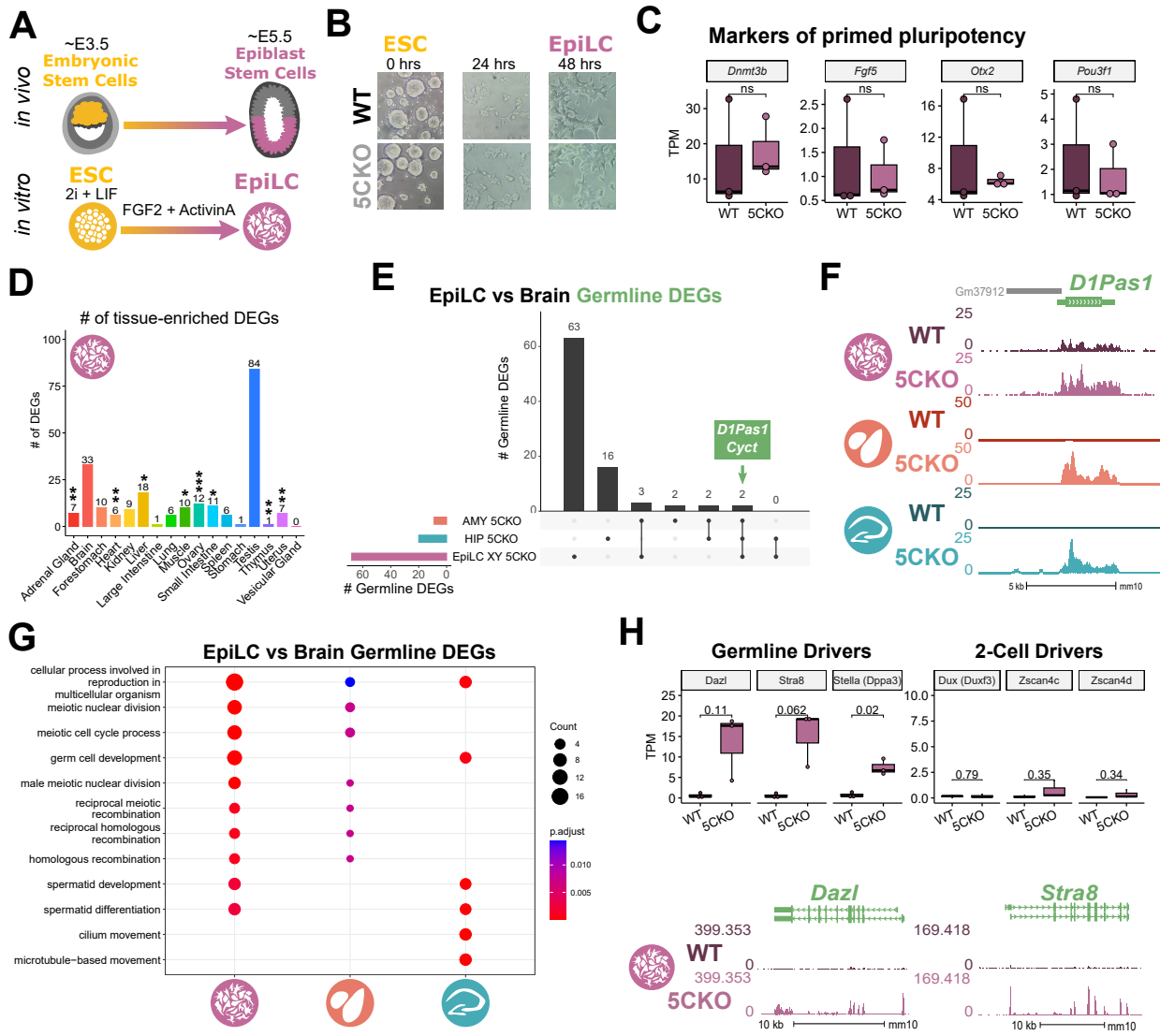


**Figure 3: Kdm5c-KO epiblast-like cells express key drivers of germline identity**

**A.** Top - Diagram of *in vivo* differentiation of embryonic stem cells (ESCs) of the inner cell mass into epiblast stem cells. Bottom - *in vitro* differentiation of ESCs into epiblast-like cells (EpiLCs).

**B.** Representative images of male wild-type (WT) and *Kdm5c*-KO (5CKO) cells during ESC to EpiLC differentiation. Brightfield images taken at 20X.

**C.** No significant difference in primed pluripotency marker expression in wild-type versus *Kdm5c*-KO EpiLCs. Welch's t-test, expression in transcripts per million (TPM).

**D.** Number of tissue-enriched differentially expressed genes (DEGs) in *Kdm5c*-KO EpiLCs, amygdala (AMY), and hippocampus (HIP) RNA-seq datasets. \*  $p < 0.05$ , \*\*  $p < 0.01$ , \*\*\*  $p < 0.001$ , Fisher's exact test.

**E.** Upset plot displaying the overlap of germline DEGs expressed in *Kdm5c*-KO EpiLCs, amygdala (AMY), and hippocampus (HIP) RNA-seq datasets.

**F.** UCSC browser view of an example germline gene, *D1Pas1*, that is dysregulated *Kdm5c*-KO EpiLCs (top, purple. Average,  $n = 3$ ), amygdala (middle, red. Average,  $n = 4$ ), and hippocampus (bottom, blue. Average,  $n = 4$ ).

**G.** enrichPlot gene ontology analysis comparing enriched biological processes for *Kdm5c*-KO EpiLC, amygdala, and hippocampus germline DEGs.

**H.** Top left - Example germline identity DEGs unique to EpiLCs. Top right - Example 2-cell genes that are not dysregulated in *Kdm5c*-KO EpiLCs. p-values for Welch's t-test. Bottom - UCSC browser view of *Dazl* and *Stra8* expression in wild-type and *Kdm5c*-KO EpiLCs (Average,  $n = 3$ ).

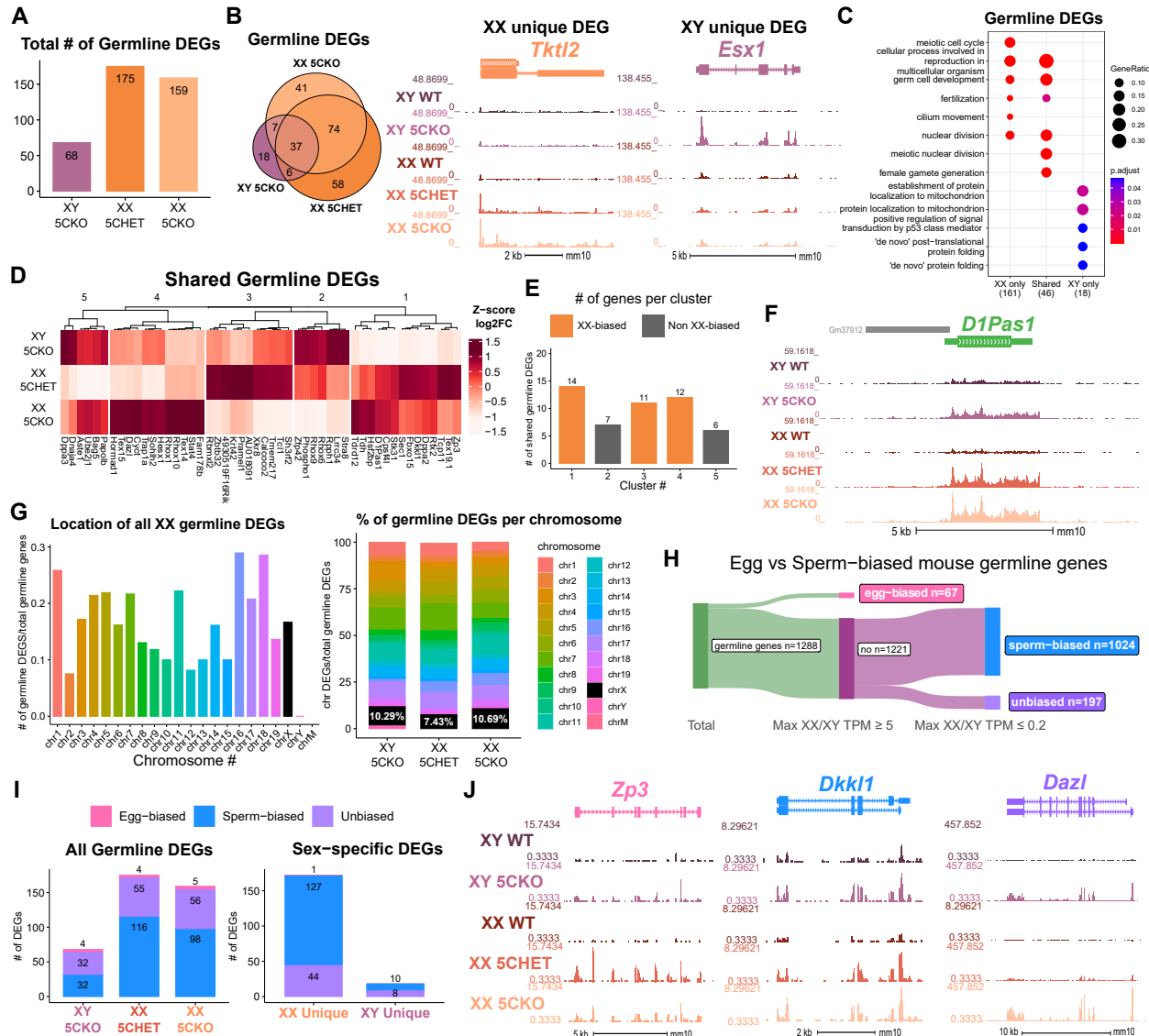


**Figure 4: Chromosomal sex influences *Kdm5c*-KO germline gene misexpression.** **A.** Total number of germline-enriched RNA-seq DEGs for male hemizygous *Kdm5c* knockout EpilCs (XY 5CKO, purple), female heterozygous *Kdm5c* knockout (XX 5CHET, orange), female homozygous *Kdm5c* knockout (XX 5CKO, light orange) EpilCs. **B.** Left - Eulerr overlap of *Kdm5c* mutant male and female EpilC germline DEGs. Right - Example of germline DEGs unique to females or males, *Tktl2* and *Esx1*. **C.** enrichPlot gene ontology analysis comparing enriched biological processes for germline DEGs shared between *Kdm5c* mutant males and females, or unique to one sex (XX only or XY only). **D.** Heatmap of germline DEGs shared between male and female mutants. Color is the average log 2 fold change from sex-matched wild-type, z-scored across rows. **E.** Number of genes within each cluster from D. Clusters with higher expression in females compared to males (XX-biased) highlighted in orange. **F.** UCSC browser view of a male and female shared germline DEG *D1Pas1* that is more highly expressed in female mutants (Average, n = 3). **G.** Left - Number of all female germline DEGs located on each chromosome over the total number of germline-enriched genes on that chromosome. Right - Percentage of germline DEGs that lie on each chromosome for each *Kdm5c* mutant. X chromosome highlighted in black. **H.** Sankey diagram classifying egg-biased (pink) and sperm-biased (blue) and unbiased (purple) mouse germline-enriched genes. **I.** Number of egg, sperm, or unbiased germline DEGs for male and female *Kdm5c* mutants. **J.** UCSC browser view of egg-biased (*Zp3*), sperm-biased (*Dkk1*), and unbiased (*Dazl*) germline genes dysregulated in both male and female *Kdm5c* mutants (Average of n = 3).

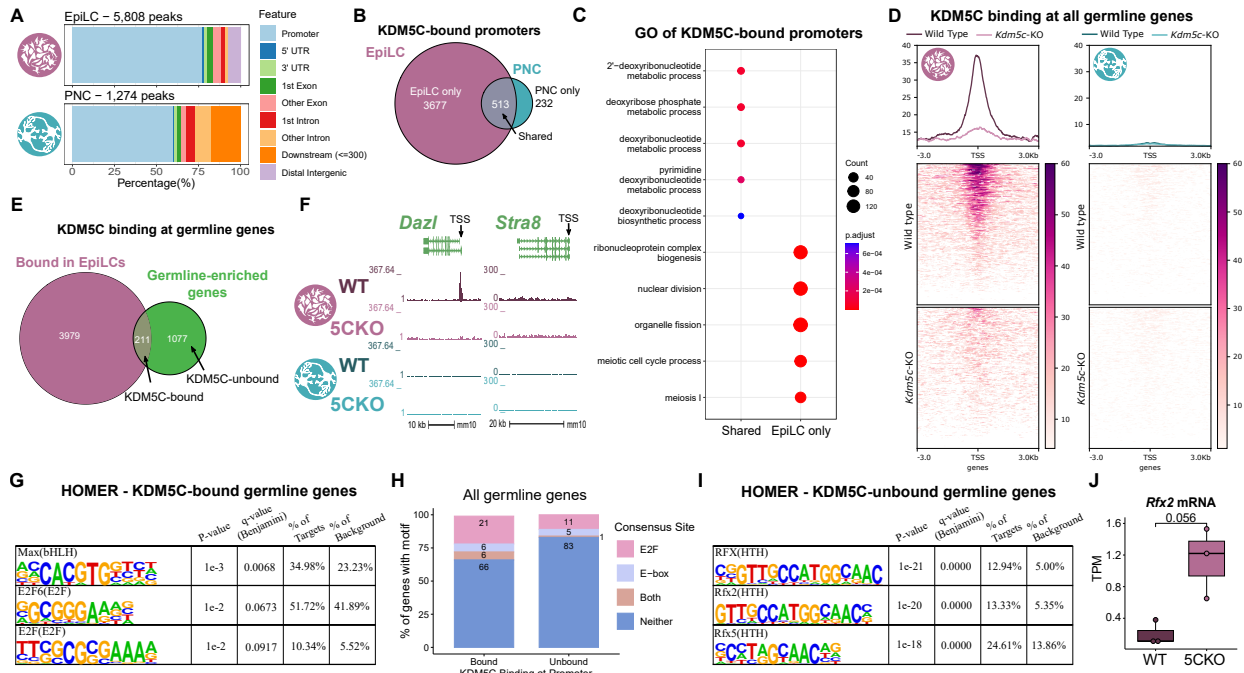


**Figure 5: KDM5C binds to a subset of germline gene promoters during early embryogenesis.** **A.** ChIPseeker localization of KDM5C peaks at different genomic regions in EpiLCs (top) and hippocampal and cortex primary neuron cultures (PNCs, bottom). **B.** Overlap of genes with KDM5C bound to their promoters ( $TSS \pm 500$ ) in EpiLCs (purple) and PNCs (blue). **C.** Gene ontology (GO) comparison of genes with KDM5C bound to their promoter in EpiLCs and PNCs. Genes were classified as either bound in EpiLCs only (EpiLC only), unique to PNCs (PNC only, no significant ontologies) or bound in both PNCs and EpiLCs (Shared). **D.** Average KDM5C binding around the transcription start site (TSS) of all germline-enriched genes in EpiLCs (left) and PNCs (right). **E.** Eulerr overlap of germline-enriched genes (green) with significant KDM5C binding at their promoter in EpiLCs (purple). **F.** Example KDM5C ChIP-seq signal around the *Dazl* TSS but not *Stra8* in EpiLCs. **G.** HOMER motif analysis of all KDM5C-bound germline gene promoters, highlighting significant enrichment of MAX, E2F6, and E2F motifs. **H.** Number of all gene promoters bound or unbound by KDM5C with instances of the E2F or E-box consensus sequence. **I.** HOMER motif analysis of all KDM5C-unbound germline gene promoters, highlighting significant enrichment of RFX family transcription factor motifs. **J.** Expression of RNA-seq DEG *Rfx2* in wild-type and *Kdm5c*-KO EpiLCs. P-value of Welch's t-test, expression in transcripts per million (TPM).

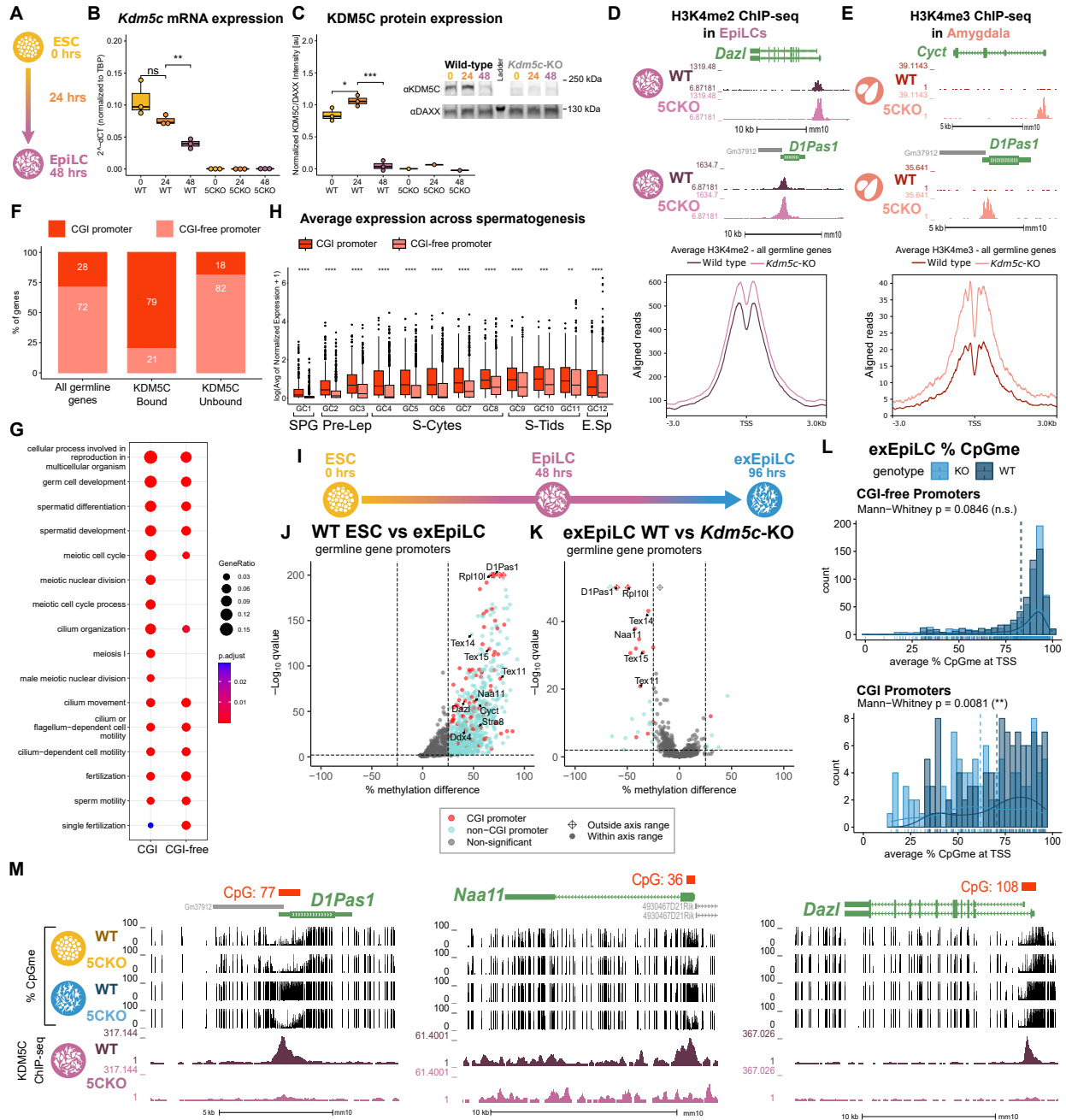


**Figure 6: KDM5C promotes long-term silencing of germline genes via DNA methylation at CpG islands.** **A.** Diagram of embryonic stem cell (ESC) to epiblast-like cell (EpiLC) differentiation and collection time points. **B.** Real time quantitative PCR (RT-qPCR) of *Kdm5c* mRNA expression in wild-type (WT) and *Kdm5c*-KO (5CKO) ESCs at 0, 24, and 48 hours of differentiation into EpiLCs. Expression calculated in comparison to TBP mRNA expression ( $2^{-\Delta\Delta CT}$ ). \*  $p < 0.05$ , \*\*  $p < 0.01$ , \*\*\*  $p < 0.001$ , Welch's t-test. **C.** KDM5C protein expression normalized to DAXX. Quantified intensity using ImageJ (artificial units - au). Right - representative lanes of Western blot for KDM5C and DAXX. \*  $p < 0.05$ , \*\*  $p < 0.01$ , \*\*\*  $p < 0.001$ , Welch's t-test. **D.** Top - Representative UCSC browser view of histone 3 lysine 4 dimethylation (H3K4me2) ChIP-seq signal at two germline genes in wild-type and *Kdm5c*-KO EpiLCs. Bottom - Average H3K4me2 signal at the TSS of all germline-enriched genes in wild-type (dark purple) and *Kdm5c*-KO (light purple) EpiLCs. **E.** Top - Representative UCSC browser view of histone 3 lysine 4 trimethylation (H3K4me3) ChIP-seq signal at two germline genes in the wild-type (WT) and *Kdm5c*-KO (5CKO) adult amygdala. Bottom - Average H3K4me3 signal at the transcription start site (TSS) of all germline-enriched genes in wild-type (dark red) and *Kdm5c*-KO (light red) amygdala. **F.** Percentage of germline genes that harbor CpG islands (CGIs) in their promoters (CGI promoter, red), based on UCSC annotation. Left - percentage of all germline-enriched genes, middle - KDM5C-bound germline genes, and right - KDM5C-unbound germline genes. (Legend continued on next page.)

**Figure 6: KDM5C promotes long-term silencing of germline genes via DNA methylation at CpG islands.** (Legend continued.) **G.** enrichPlot gene ontology analysis of germline genes with (CGI-promoter) or without (CGI-free) CGIs in their promoter. **H.** Expression of germline genes with (CGI-promoter, red) or without (CGI-free, salmon) CGIs in their promoter across stages of spermatogenesis from Green et al 2018. SPG - spermatogonia, Pre-Lep - preleptotene spermatocytes, S-Cytes - meiotic spermatocytes, S-Tids - post-meiotic haploid round spermatids, E.Sp - elongating spermatids. Wilcoxon test, \*  $p < 0.05$ , \*\*  $p < 0.01$ , \*\*\*  $p < 0.001$ , \*\*\*\*  $p < 0.0001$ . **I.** Diagram of ESC to extended EpiLC (exEpiLC) differentiation. **J.** Volcano plot of whole genome bisulfite sequencing (WGBS) comparing CpG methylation (CpGme) at germline gene promoters ( $TSS \pm 500$ ) in wild-type (WT) ESCs versus exEpiLCs. Significantly differentially methylated promoters ( $q < 0.01$ ,  $|methylated difference| > 25\%$ ) with CGIs in red, CGI-free promoters in light blue **K.** Volcano plot of WGBS of wild-type (WT) versus *Kdm5c*-KO exEpiLCs for germline gene promoters. Promoters with CGIs in red, CGI-free promoters in light blue. **L.** Histogram of average percent CpGme at the promoter of germline genes with or without CGIs. Wild-type in navy and *Kdm5c*-KO (KO) in light blue. Dashed lines are average methylation for each genotype, p-values for Mann-Whitney U test. **M.** UCSC browser view of germline genes, showing UCSC annotated CGI with number of CpGs, representative CpGme in wild-type (WT) and *Kdm5c*-KO (5CKO) ESCs and exEpiLCs, and KDM5C ChIP-seq signal in EpiLCs.